Defence Research and Development Canada
Recherche et développement pour la défense Canada

DEFENCE R&D DÉFENSE

Short-range bioaerosol LIDAR detection: transmitter design and sensitivity analysis

J.-R. Simard
DRDC Valcartier

Defence R&D Canada – Valcartier
Technical Memorandum
DRDC Valcartier TM 2005-303
August 2006

Canada

Short-range bioaerosol LIDAR detection: transmitter design and sensitivity analysis

J.-R. Simard
DRDC Valcartier

Defence R&D Canada - Valcartier

Technical Memorandum

DRDC Valcartier TM 2005-303

August 2006

Auteur

Jean-Robert Simard

Approuvé par

Jean-Marc Garneau
Chef de Section

Approuvé pour publication par

Gilles Bérubé
Scientifique en chef

Abstract

With the decline of the traditional worldwide balance of power between the major alliances since the early 1990s, and the concurrent rise of asymmetric threats, biological warfare has been identified as and still is one of the threats for which adequate defences are the most challenging. One recently identified need is a short-range volumetric bioaerosol sensor capable of monitoring large indoor or semi-enclosed outdoor spaces. In response to this interest, DRDC – Valcartier investigated the potential of a miniature inelastic short-range LIDAR (the Short-Range BioSpectra concept). In addition to addressing the identified deficiencies, this device would also accelerate the potential assessment of classifying biological aerosols from the spectral information contained in their induced fluorescence. In this study, several modelling considerations necessary for an efficient short-range LIDAR transmitter design are reported. From this model, the present state of the technologies and previously obtained scattering properties of a bioaerosol simulant (BG), sensitivities varying from less than 1 to about 80 ACPLA, are anticipated for ranges varying from 5 to 50 metres and collecting apertures of 5, 10, 15 and 20 cm in diameter. This level of sensitivity is obtained for probed range intervals of less than .5 m to over 30 m and delimiting atmospheric volumes varying from a fraction of a millilitre up to 60 mL. These results are supplemented with discussions on issues like the limit of validity of the proposed model, the modelling of background parasitic signals, preprocessing requirements, possible parasitic fluorescence sources (an issue that must be overcome in order to achieve the reported sensitivity predictions), and how to interpret the concentration sensitivity of a bioaerosol detector based on LIDAR technology.

Résumé

Avec le déclin de l'équilibre existant entre les superpuissances mondiales qui s'est déroulé depuis le début des années 90 et l'accroissement des menaces asymétriques qui a été observé en parallèle, les armes biologiques ont été identifiées comme une des menaces pour laquelle une défense adéquate représente un important défi. Un besoin identifié récemment est un détecteur volumétrique à courte distance d'aérosols biologiques pour la surveillance de vastes espaces fermés ou semi-fermés. En réponse à cet intérêt, RDDC Valcartier a évalué le potentiel d'un LIDAR miniature inélastique à courte portée (le concept 'Short-Range BioSpectra'). En plus de s'attaquer au problème soulevé, ce dispositif permettra aussi d'accélérer l'évaluation du potentiel de classification des aérosols biologiques à partir de l'information spectrale contenue dans leur fluorescence induite. Dans cette étude, plusieurs considérations reliées au modèle pour le design d'un transmetteur LIDAR efficace sont rapportées. À partir de ce modèle, de l'état présent de la technologie et des caractéristiques de diffusion de simulant de bioaérosol (BG) obtenues de précédents travaux, des niveaux de détections minimums variant de moins de 1 jusqu'à 80 ACPLA sont anticipés pour des distances allant de 5 à 50 mètres et des ouvertures optiques de 5, 10, 15 et 20 cm de diamètre. Ces niveaux de détection sont obtenus pour des intervalles en distance de moins de un demi-mètre jusqu'à plus de 30 mètres. Ces intervalles correspondent à des volumes atmosphériques variant d'une fraction de 1 millilitre jusqu'à environ 60 millilitres. Ces résultats sont complétés par une discussion sur des aspects comme la limite de validité du modèle, la modélisation des signaux parasitaires de fond, la nécessité du prétraitement des acquisitions, de possibles

sources de fluorescence parasitaire (une difficulté potentiellement importante à minimiser afin d'atteindre les limites de détections présentées) et comment interpréter une limite de détection en concentration pour un détecteur de bioaérosols basé sur la technologie LIDAR.

Executive summary

With the decline of the traditional worldwide balance of power between the major alliances since the early 1990s, and the concurrent rise of asymmetric threats, biological warfare has been identified as and still is one of the threats for which adequate defences are the most challenging. The traditional approach to addressing this menace is based on the use of (an array of) point detectors. However, this technique has considerable limitations in monitoring wide-open areas. To overcome these limitations, DRDC investigated spectrometric intensified range-gated detection of laser-induced fluorescence of bioaerosols (SINBAHD project, 1999-2002), a concept associated with Light Detection and Ranging (LIDAR) technologies. This study demonstrated sensitivity levels at multi-kilometre distances of a few Agent Containing Particles per Litre of Air (ACPLA) and a significant classification potential associated with the spectral information contained within the induced fluorescence originating from the bioaerosols.

More recently, the need for a short-range volumetric bioaerosol sensor capable of monitoring large indoor and semi-enclosed outdoor spaces has been identified. A Broad Agency Announcement (BAA) published by the US Homeland Security Advanced Projects Agency (HSARPA) for Instantaneous Bio-Aerosol Detector Systems (IBADS) is one example of this emerging requirement. In response to this interest, DRDC – Valcartier investigated the potential of a miniature inelastic LIDAR based on the SINBAHD concept. In addition to having a strong potential for efficiently addressing the requirements associated with the monitoring of large indoor and semi-enclosed outdoor spaces, this miniature spectrometric LIDAR would also accelerate the assessment of the potential of classifying bioaerosols based on the analysis of the spectral information contained in their induced fluorescence. The initial effort associated with this work has produced the concept known as Short-Range BioSpectra (SR-BioSpectra) registered as a Report of an Invention.

To assess the potential of the SR-BioSpectra concept, several modelling considerations are presented. The fundamental LIDAR model is re-visited and adapted for a short-range transmitter design. The optical design of SR-BioSpectra, including its innovative fibre bundle module, is detailed. The geometrical form factor, a key parameter for an efficient LIDAR transmitter, is assessed. The basic principles associated with the background parasitic signal dictating the sensitivity limit of the instrument are characterized. Based upon the scattering properties of *Bacillius Globiggi* (BG) obtained from the lessons learned in the SINBAHD project, a sensitivity varying from less than 1 to about 80 ACPLA is anticipated for ranges varying from 5 to 50 m and collecting apertures of 5, 10, 15 and 20 cm in diameter. These sensitivity results show that monitoring background fluorescing aerosols, commonly between 1 and 100 ACPLA, are within reach, making this a promising technology for operational bioaerosol monitoring applications. To achieve this level of sensitivity, the probed range intervals, delimiting monitored atmospheric volumes varying from a fraction of a millilitre to about 60 mL, correspond to from less than .5 m to over 30 m. These results are supplemented with a discussion on issues like the limit of validity of the proposed model, the modelling of the background parasitic signal (usually dictating the sensitivity limit), the requirement for preprocessing the acquired spectra, possible parasitic fluorescence sources (an issue that must be overcome in order to achieve the reported sensitivity predictions), and how to interpret the concentration sensitivity of a bioaerosol detector based on LIDAR technology.

In summary, the predicted capabilities of a short-range volume biodetector reported in this memorandum support future efforts to develop a breadboard demonstrator that will allow these results to be verified experimentally based on the proposed model.

Simard, J.-R., 2005.
Short-range Bioaerosol LIDAR detection: transmitter design and sensitivity analysis.
[DRDC – Valcartier TM 2005-303] Defence R&D Canada – Valcartier.

Sommaire

Avec le déclin de l'équilibre existant entre les superpuissances mondiales qui s'est déroulé depuis le début des années 90 et l'accroissement des menaces asymétriques qui a été observé en parallèle, les armes biologiques ont été identifiées comme une des menaces pour laquelle une défense adéquate représente toujours un important défi. L'approche traditionnelle pour solutionner cette menace est basée sur l'utilisation de (d'un réseau de) détecteurs ponctuels. Toutefois, cette technique a d'importantes limites dans le cas de surveillance de grands espaces ouverts. Afin de réduire ces limites, RDDC a étudié la détection spectrale de fluorescence induite par laser provenant d'aérosols biologiques et basée sur une intensification à crénelage (projet SINBAHD, 1999-2002), un concept relié à la technologie LIDAR ('Light Detection and Ranging'). Cette étude a démontré des niveaux de détection minimale de quelques ACPLA ('Agent Containing Particle per Liter of Air') à des distances multi kilométriques et un important potentiel de classification à partir de l'information spectrale contenue dans la fluorescence induite provenant de ces bioaérosols.

Récemment, le besoin pour un détecteur volumétrique d'aérosols biologiques à courte portée capable de surveiller de vastes espaces fermés ou semi-ouverts sur l'extérieur a été identifié. Un 'Broad Agency Announcement (BAA)' publié par le 'US Homeland Security Advanced Projects Agency (HSARPA)' pour un 'Instantaneous Bio-Aerosol Detector Systems (IBADS)' est un exemple de ce besoin émergent. En réaction à cet intérêt, DRDC Valcartier a étudié le potentiel associé à un LIDAR inélastique miniature basé sur le concept SINBAHD. En plus de présenter un fort potentiel à résoudre efficacement les besoins associés à la surveillance de vastes espaces fermés et semi-fermés, ce LIDAR spectrométrique miniature pourrait aussi accélérer l'évaluation du potentiel de la classification des aérosols biologiques basée sur l'analyse de l'information spectrale contenue dans leur fluorescence induite. L'effort initial associé à ce travail a produit le concept intitulé 'Short-Range BioSpectra (SR-BioSpectra)' et a fait l'objet d'un Rapport d'Invention.

Afin d'évaluer le potentiel du concept SR-BioSpectra, plusieurs considérations reliées au modèle proposé sont présentées. Le modèle fondamental du LIDAR est re-visité et adapté au design d'un transmetteur à courte portée. Le facteur géométrique d'obscuration, un paramètre clé pour un transmetteur LIDAR efficace, est analysé. Les principes de base associés au signal parasitaire de fond dictant la limite de détection de l'instrument est caractérisés. En introduisant les propriétés de diffusion du *Bacillius Globiggi* (BG) obtenues de leçons apprises avec le projet SINBAHD, une limite de détection variant de moins de 1 à 80 ACPLA est anticipée pour des portées variant de 5 à 50 mètres et des ouvertures de collections de 5, 10, 15 et 20 cm de diamètre. Ces niveaux de détection minimum sont obtenus en mesurant la fluorescence provenant d'échantillons volumiques variant de moins d'un millilitre à près de 60 millilitres distribués sur des intervalles en porté variant de moins d'un demi-mètre à plus de 30 mètres. Ces résultats sont complétés par une discussion sur des aspects comme la limite de validité du modèle proposé, la modélisation du signal parasitaire de fond dictant habituellement la limite de détection, la nécessité de traiter au préalable les acquisitions spectrales, les possibles sources de fluorescence parasitaires (un aspect important à étudier afin d'obtenir les prédictions de détection minimale rapportées) et comment interpréter une détection minimale exprimée en concentration pour un détecteur d'aérosol biologique basé sur la technologie LIDAR.

En perspective, les capacités prédites associées à un détecteur volumique à courte portée d'aérosols biologiques qui sont rapportées dans ce mémorandum supportent futurs efforts afin de développer un démonstrateur de concept qui permettra de vérifier expérimentalement les résultats obtenus avec le modèle développé.

Simard, J.-R., 2005.
Short-range bioaerosol LIDAR detection: transmitter design and sensitivity analysis,
[RDDC Valcartier TM 2005-303] R&D pour la Défense Canada – Valcartier.

Table of contents

This page is left blank intentionally.

List of figures

List of tables

This page is left blank intentionally.

1. Introduction

With the decline of the traditional worldwide balance of power between the major alliances since the early 1990s, and the concurrent rise of asymmetric threats, biological warfare has been identified as and still is one of the threats for which adequate defences are the most challenging. Up to the end of the 1990s, the major efforts to address this threat were based on point biological detectors. The main drawback of this technological approach is that a point detector must be within a cloud of bioagents to detect it. This may not be a problem if the asset being monitored is a key narrow space such as the main ventilation room of a building. However, an approach based on (an array of) point detectors has significant limitations where a wide-open area needs to be monitored for bioaerosol threats. These limitations result from the large number of detectors required to efficiently cover a multi-square-kilometre zone and their (presently excessive) unit price[1]. To overcome this deficiency, standoff biodetectors based on LIDAR technologies have been investigated. Such techniques, based on the elastic and inelastic scattering properties of bioaerosols, have demonstrated sensitivities and classification potentials suitable for long-range biothreat monitoring. For instance, the SINBAHD system (Ref. 1), using a LIDAR based on the gated spectrometric detection of intensified laser-induced fluorescence, has demonstrated sensitivity of a few bioaerosols per litre of air at multi-kilometre distances and a promising potential for recognizing the type of bioaerosol based on the spectral information contained in the detected fluorescence.

More recently, the need for a short-range volumetric bioaerosol sensor capable of monitoring large indoor and semi-enclosed outdoor spaces has been identified. The Broad Agency Announcement 04-18 (BAA-04-18) published by the US Homeland Security Advanced Projects Agency (HSARPA) for Instantaneous Bio-Aerosol Detector Systems (IBADS) is one example of this emerging requirement. In response to this interest, DRDC – Valcartier investigated the potential of a miniature inelastic LIDAR based on the SINBAHD concept. In addition to having strong potential for addressing the requirements associated with the monitoring of large indoor and semi-enclosed outdoor spaces, this miniature spectrometric LIDAR would also accelerate the assessment of classifying bioaerosols by analyzing the spectral information contained in their induced fluorescence. The initial effort associated with this work has produced the concept referred to as Short-Range BioSpectra (SR-BioSpectra) registered in a Report of an Invention (Ref. 2). In support of this initial effort, this memorandum describes the model predicting the sensitivity of the SR-BioSpectra concept based on the lessons learned in the SINBAHD project.

Even if it is anticipated that the spectrometric detection components of the SR-BioSpectra concept and the SINBAHD device would be fairly similar, important

1 Commercially available point bioaerosol detectors presently cost well over $100,000 each, and their price reduction to an amount compatible with efficient wide area monitoring is not forseen in the near future.

differences are anticipated in their optical transmitters. For either short- or long-range LIDARs, the transmitter generates a narrow beam of short but intense light pulses (usually produced with a laser) and collects the light scattered by aerosols and gases along its path. For long-range applications, the transmitter is usually configured for far-field detection, making the system optically efficient from a minimum range to infinity, where the return signal is recorded as a function of time. This long-range configuration also has the advantage of using a narrow collection field of view, an important requirement for minimizing background radiance contribution, while avoiding a geometric obscuration penalty over this extended range interval of detection. For short-range LIDAR where a narrow field of view is still necessary, basic geometric principles greatly limit the minimum range of operation of a transmitter based on this approach. In order to overcome the difficulty of combining a narrow field of view with an efficient transmitter for short-range LIDAR design, the image plane of the transmitter must be displaced from infinity to the range of interest. Locating the conjugated image of the transmitter at a given short range has the disadvantage of limiting the efficient sensing volume to within a narrow range interval centred at that image position. Under this short-range design, a signal distributed as a function of range loses its usefulness. Nevertheless, the loss of the signal distributed as a function of range that is associated with the classical long-range LIDAR design has little impact for the applications pursued with the SR-BioSpectra concept. With this approach, the induced fluorescence that is analyzed spectrally will originate from a single range interval in any case.

This document reports several modelling considerations for an efficient short-range LIDAR transmitter design. In Section 2, it re-visits the fundamental concepts defining the amplitude of the signal collected by a LIDAR and adapts these principles for short-range transmitter designs. In Section 3, the SR-BioSpectra concept is detailed, followed by the analysis of its geometric form factor. Then, the laser irradiation geometry resulting from fibre bundle technologies is examined. Next, the principles allowing the comparison of sensitivity between the SR-BioSpectra concept and the SINBAHD device are established, and the background radiance (dictating in large part the sensitivity of LIDAR devices) is modelled. In Section 4, the previously developed model and the lessons learned in the SINBAHD project are combined to predict the sensitivity of SR-BioSpectra as a function of range and the size of the collection optics. In addition to sensitivity, other issues like the range interval and the sampling volume are also analyzed as a function of the same parameters. Section 5 presents a discussion on several issues like the limits of validity of the proposed model, background radiance, parasitic fluorescence, preprocessing requirements and understanding the sensitivity of LIDAR devices. Finally, a conclusion highlights the main contributions of this document.

This study, made possible with the discretionary support of DRDC – Valcartier to assess the potential of standoff biodetection, was conducted between April 2002 and March 2005.

2. Model description

Before predicting the capacity of a short-range inelastic LIDAR design, it is important to re-visit the fundamental model associated with LIDAR devices. This will be done in Section 2.1 and is in large part inspired from Measures (Ref.3). Then, this fundamental model will be detailed further in Section 2.2 for the specific case of short-range inelastic LIDARs.

2.1 Fundamentals

At the fundamental level, the optical signal collected by all LIDARs can be defined as a differential equation relating the element of light collected and sent to a detector and the element of volume from where this light originated. This equation can be expressed as

$$dP_\lambda(\lambda_0,\vec{r},t) = J_\lambda(\lambda_0,\vec{r},t)\, p_\lambda(\vec{r})\, dV\,, \tag{1}$$

where dP_λ is the spectral element of light power detected at a time t resulting from elastic or inelastic scattered laser light with an excitation wavelength λ_0[2] and within a volume element dV located at position $\vec{r}$, $J_\lambda(\lambda_0,\vec{r},t)$ is the spectral radiance generated by the scattered laser light within that volume dV and responsible for the detected spectral element of light[3] and $p_\lambda(\vec{r})$, the geometric factor, is the fraction of this spectral radiance that reaches the LIDAR detector. For the work reported here, only the inelastic scattered laser light will be discussed further. However, the model developed here can easily be adapted to elastic scatters.

The spectral radiance J_λ is detailed by introducing the laser irradiance I incident at the volume dV as

$$J_\lambda(\lambda_0,\vec{r},t) = \beta_\lambda(\lambda_0,\vec{r})\, I(\lambda_0,\vec{r},t)\,, \tag{2}$$

where β_λ is defined as the volume spectral backscattering coefficient at position $\vec{r}$. This coefficient takes into account the physical characteristics of the scatters and depends on the excitation wavelength. It can be defined as

---

2 Here, it is considered that the laser light is monochromatic and centered at wavelength λ_0. This definition could be generalized for multi-wavelength or white lasers. However, the increased level of complexity generated by this additional step of generalization is not necessary for the subject discussed in this report.

3 It is important to note the time delay that exists between the moment where the spectral radiance is generated within the volume element dV and the moment it is detected by the LIDAR. This delay corresponds to the time of flight between this volume element and the LIDAR. This variable will be introduced as eq.1 is detailed further in the following discussion.

$$\beta_\lambda(\lambda_0,\vec{r}) = \sum_i \mathrm{N}_i(\vec{r})\,\sigma_\lambda^i(\lambda_0)\,, \tag{3}$$

where $\mathrm{N}_i(\vec{r})$ is the volume density of scatter *i* at position $\vec{r}$ and σ_λ^i is the spectrally distributed inelastic backscattering cross section of scatter species *i* for an excitation wavelength λ_0.

In order to detail further the inelastic cross section, two assumptions must be introduced. First, the quantum yield of the scatter species i, Ψ_i, expressing its efficiency to produce inelastic photons[4] and the inelastic spectral probability density ζ_λ^i, the probability that an inelastic scattered photons is generated within a spectral interval centered at a wavelength λ, are independent of the projected area[5] of the scatter i, A_i, when submitted to the incident laser irradiance. Second, the scatters emit the inelastic photons in all directions with the same probability. With these assumptions, the spectrally distributed inelastic scattering cross section of specie *i* is defined as

$$\sigma_\lambda^i(\lambda_0) = \frac{\Psi_i(\lambda_0)\,\mathrm{A}_i}{4\pi}\zeta_\lambda^i(\lambda_0)\,. \tag{4}$$

Finally, the geometric factor $p_i(\vec{r})$ introduced in Eq.1 can be detailed further as

$$p_\lambda(\vec{r}) = \frac{\mathrm{A}_{AS}}{\left|\vec{r}\right|^2} \times t_\lambda^a(\vec{r}) \times t_\lambda^o(\vec{r}) \times \xi(\vec{r})\,, \tag{5}$$

where A_{AS} is the area of the aperture stop of the collecting optics, t_λ^a and t_λ^o are the atmospheric and transmitter spectral transmission, respectively, for a collected photon originating from location $\vec{r}$. $\xi(\vec{r})$ is the overlap function describing the fraction of scattered photons emitted at location $\vec{r}$ and collected by the aperture stop that will be detected by the detector. This last parameter is regularly referred as the geometrical form factor or obscuration factor. This parameter is also expressing the main criteria to optimize for an adequate optical design of a LIDAR transmitter.

Eqs. 1-5 form the fundamental model of most spectrometric LIDAR designs. Only two basic assumptions have been inserted to obtain this basic model: the mutual independence of the cross section variables in Eq.4 and the isotropic probability of the

---

4 The quantum yield Ψ_i can be defined as the ratio of inelastic photons produced for a given number of incident excitation photons interacting with scatter *i*.

5 The projected area can be seen as an equivalent planar surface occupying the field of view associated to the scatter as seen by the LIDAR transmitter.

direction taken by induced inelastic photons. In the following Section, this basic model will be refined further for the specific case of short-range LIDAR design.

2.2 Applying the basic LIDAR model to short-range applications

The signal detected by a LIDAR results from the integration of all the spectral elements of scattered light defined by Eq.1 and reaching the detector at a given time *t*. This is expressed as

$$P_\lambda(\lambda_0,t) = \int_V dP_\lambda(\lambda_0,\vec{r},t) = \int_V J_\lambda(\lambda_0,\vec{r},t)\, p(\lambda,\vec{r})\, dV \,, \tag{6}$$

where the integrated volume is the entire space surrounding the LIDAR instrument. However, since the spectral radiance results from the laser irradiance (see Eq.2), V is in fact limited to the volume where the laser irradiance is not negligible. Based on the irradiating laser beam geometry, it is advantageous to use the cylindrical coordinate system to solve Eq.6. This allows expressing $\vec{r}$ as $\vec{z} + \vec{r}_c$ where $\vec{z}$ is the coordinate along the optical axis defined by the LIDAR transmitter (and the laser beam when co-aligned) and $\vec{r}_c$ is the radial coordinate in a plane perpendicular to that optical axis.

For the variables embedded in Eq.6 that depend essentially on the traveled distance made by the photons as the atmospheric transmission and the inverse square law dictating the amplitude of a free expanding wave, the variable $\vec{r}$ reporting the location of the volume element can be approximated by z ($z = |\vec{z}| \approx |\vec{r}|$) as long as $|\vec{r}_c| << z$. This reduces $p_\lambda(\vec{r})$ defined by Eq.5 to

$$p_\lambda(\vec{r}) = \frac{A_{AS}}{z^2} \times t_\lambda^a(z) \times t_\lambda^o \times \xi(\vec{r}) \,. \tag{7}$$

In this result, the transmission of the collecting optics t_λ^o has also been approximated as independent of $\vec{r}$. This is reasonable since this parameter should vary little with the optical entrance path in the transmitter. However, for the precise evaluation of the spectral probability density ζ_λ^i associated with specie *i*, this approximation may require revisiting, particularly with a transmitter design not based on cylindrical symmetry. Another important approximation can be introduced for short-range LIDAR applications with a range of visibility much greater than the LIDAR range of operation (this is particularly true in the visible spectrum where little atmospheric chemical absorption spectral structure exists). In this case, $t_\lambda^a(z)$ can be approximated as unity.

Combining Eqs.2, 3, 4, 7 and the previously stated approximations in Eq.6 allows the expression of the signal detected by the LIDAR for a single scatter *i* as follows

$$P_\lambda^i(\lambda_0,t) =$$

$$\frac{\mathrm{A}_{AS}\, t_\lambda^o \Psi_i(\lambda_0)\mathrm{A}_i \zeta_\lambda^i(\lambda_0)}{4\pi} \int_0^{z=ct/2} \left[\frac{1}{\mathrm{z}^2} \left[\iint \xi(z,\vec{r_c})\,\mathrm{N}_i(z,\vec{r_c})\, I(\lambda_0,z,\vec{r_c},t)\, d\mathrm{A} \right] \right] \otimes u_i(c\tau)\, dz\,. \qquad (8)$$

In this equation, the speed of light c has been introduced to take into account the delay caused by the time of flight between the volume element at the origin of the scattered photons and the LIDAR detector. Furthermore, the convoluting expression $u_i(c\tau)$ has been introduced for the scatter i to take into account the non-instantaneous conversion of the laser irradiation into inelastic scattered photons[6]. In this equation, u_i is the function expressing the impulse response of the inelastic conversion process and τ is an independent variable describing the time evolution of this conversion process.

The parameter $ct/2$ as the upper limit in the range integration of Eq.8 takes into account time delay associated with the simultaneous detection of each scattered signal originating from the different volume elements distributed along the z-axis. It first takes into account the time needed by the laser irradiation to reach the volume element and second, the time needed by the scattered photons to reach the LIDAR detector on their return path.

In order to reduce the complexity of Eq.8 to a formulation easier to interpret for most scenarios of interest while keeping an acceptable accuracy, additional approximations are introduced. First, the laser irradiating pulses are approximated as having a square duration τ_p. Second, the dynamic shape of the inelastic conversion process is also approximated as square with a duration process τ_f[7]. These two approximations allow reducing the integration along z in Eq.8 only to the range interval defined by the position and length of the laser pulse extended by the non-instantaneous inelastic conversion time, a result originating from the convolution process. Thirdly, the laser irradiation I in a plane perpendicular to the optical axis is approximated as constant over a cylindrical area $A_L(z)$ representing the laser cross-area and zero elsewhere. These approximations have two impacts on Eq.8. First it reduces the integration area of the embedded integral to $A_L(z)$, the area where laser irradiation is not zero. Second, it allows the derivation of the irradiance I after convolution process as $E_L/\left((\tau_p+\tau_f)A_L(z)\right)$ where E_L is the energy of the laser pulse. Finally, a last approximation is introduced by assuming an uniform concentration of scatter N_i within the volume defined by the laser pulse duration times its cross area

6 Fluorescence of bioaerosol, as most fluorescence phenomenon, is very fast, usually of the order of a few nanoseconds. However, since laser pulse duration are comparable, the fluorescence time dynamic must be included in eq.8.

7 The index f is used here as a reference to fluorescence interactions. However, even if fluorescence represents most cases of interest associated with spectrometric LIDAR, the presented formulation is not limited solely to this inelastic phenomenon.

$c\tau_p A_L$ [8]. With these approximations, the power detected as a function of time given by Eq.8 is reduced to

$$P_\lambda^i(\lambda_0,t)=\frac{\mathrm{A_{AS}}\,t_\lambda^o\Psi_i(\lambda_0)\mathrm{A}_i\zeta_\lambda^i(\lambda_0)\mathrm{N}_iE_L}{4\pi(\tau_f+\tau_p)}\int_{z=^{c(t-\tau_f-\tau_p)}/_2}^{z=^{ct}/_2}\frac{1}{\mathrm{z}^2}\left[\iint_{A_L(z)}\frac{\xi(z,\vec{r}_c)}{A_L(z)}\;d\mathrm{A}\right]dz\,. \tag{9}$$

In practice, a LIDAR detector will report the total signal detected within the resolved time interval. This time interval could be determined by the bin resolution of a transient detector, as it is the case for classical LIDAR designs. However, for the case of spectrometric LIDARs similar to the SR-BioSpectra concept described in the following chapter, the time interval is determined by the gate duration Δt of an intensified charge coupled device (or ICCD). With this definition, the spectral energy detected by a LIDAR within a time interval Δt is defined as

$$E_\lambda^i(R,\Delta t,\lambda_0)=\int_{2R/c}^{2R/c+\Delta t}P_\lambda^i(\lambda_0,t)\;dt \tag{10}$$

where $2R/c$ is the time delay applied before collecting the scattered return from a range bin starting at R[9] and extending up to range interval depending in part on the duration Δt of the gate width but also on the laser pulse width τ_p and the non-elastic scattering conversion response time of scatter i τ_f.

By inserting Eq.9 in Eq.10, the spectral energy detected is re-written as

$$E_\lambda^i(R,\Delta t,\lambda_0)=\frac{\mathrm{A}_{AS}\,t_\lambda^o\,\Psi_i(\lambda_0)\mathrm{A}_i\,\zeta_\lambda^i(\lambda_0)\mathrm{N}_i\,E_L}{4\pi(\tau_f+\tau_p)}\,\Phi(R,\Delta t) \tag{11}$$

where $\Phi(R,\Delta t)$, the parameter quantifying the integration of all inelastic scattered photons from scatter i within a range bin starting at R and a range interval resulting from an integration time Δt, is derived as

$$\Phi(R,\Delta t)=\int_{2R/c}^{2R/c+\Delta t}\left[\int_{z=^{c(t-\tau_f-\tau_p)}/_2}^{z=^{ct}/_2}\frac{1}{\mathrm{A}_L(z)\,\mathrm{z}^2}\left[\iint_{A_L(z)}\xi(z,\vec{r}_c)\;d\mathrm{A}\right]dz\right]dt\,. \tag{12}$$

---

8 With complex cloud spatial distribution, this is equivalent to approximate N_i as the averaged scatter aerosol concentration within that volume.

9 The variable *R*, equivalent to *z*, is introduced to differentiate the range of detection from the range of integration of the LIDAR parameters defining P_λ^i.

3. Interpreting the short-range LIDAR model for spectrometric bioaerosol detection

In the previous Chapter, fundamentals of LIDAR theory have been reviewed and adapted for gated short-range LIDAR designs. In the following, these fundamental concepts will be applied to the SR-BioSpectra concept. First, SR-BioSpectra is detailed schematically. Then, its optical design is analyzed in order to characterize the geometrical form factor of the transmitter. To complete this analysis, the laser irradiation geometry produced by the fiber bundle module is also modeled. The following Section establishes the basic concepts allowing sensitivity comparison between the SR-BioSpectra concept and the SINBAHD device. Finally, the background parasitic signal, the main quantity dictating the sensitivity of a LIDAR, is detailed.

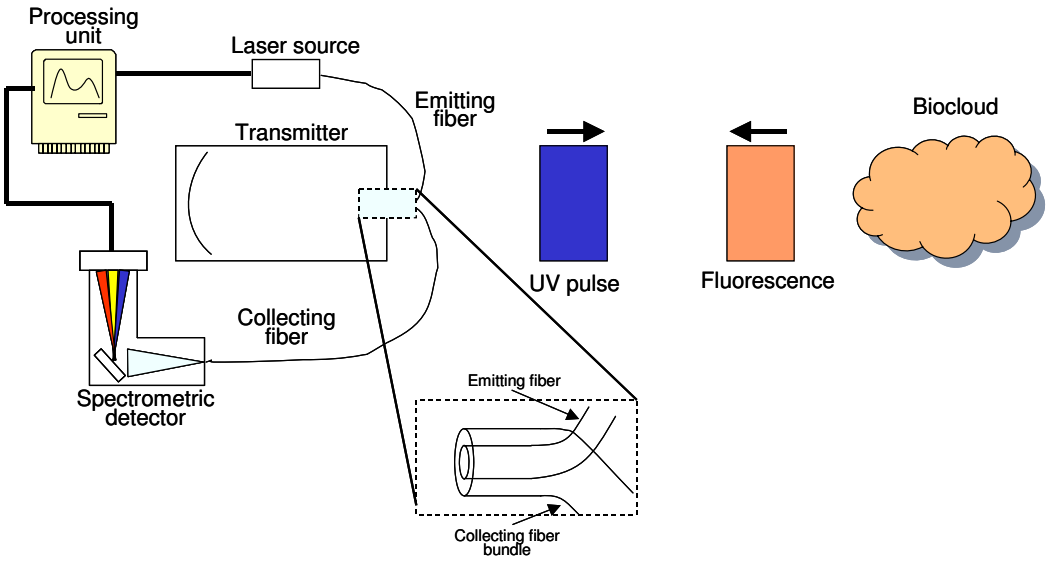

Fig.1 Schematic description of the short-range BioSpectra concept. This spectrometric LIDAR is composed of five main components: the UV laser source, the transmitter, the injection/collection module based on fiber bundle technology, the spectrometric detector and the processing unit. Such system probed the surrounding open-air for UV laser induced fluorescence originating from aerosolized materials of biological origin. It takes advantage of the compactness of fiber optic technologies and exploits the spectral information contained in the detected fluorescence to discriminate the possible types of fluorescing aerosols at the origin of the detected signal.

3.1 Description of a short-range spectrometric inelastic LIDAR: the SR-BioSpectra

The SR-BioSpectra concept has been reported in a declaration of invention (Ref.2). A schematic description of the physical components of this LIDAR concept is displayed in Fig.1. It is composed of a UV laser firing short pulses that are injected in

the transmitter via a single mode fiber optic. This UV irradiance is directed toward the image plane of the single mode fiber made by the transmitter and where the presence of threatening bioaerosols must be assessed[10]. If bioaerosols are present, inelastic scattering is generated and part of this signal is returned at the transmitter. This inelastic scattering results essentially from Raman interaction with atmospheric main gases and fluorescence from bioaerosols and other atmospheric inelastic scatterers (gases or aerosols) having resonant transitions with the incident UV irradiance. The inelastic scattering collected by the transmitter is coupled to a fiber bundle surrounding the emitting single mode fiber. It is important to note that not all scattered photons are returned at the emitting fiber. This would be the case if all these photons originated from the fixed range corresponding to the image plane of the single mode fiber. However, since the scatters are distributed as a function of range (they are out of focus), the scattered photons will form a blur centered on the single mode emitting fiber. The size and distribution of this blur, or said otherwise, the efficiency of collection of such transmitter design based on a fiber bundle can be derived by solving Eq.11 for this specific geometry. The signal gathered by the fiber bundle is directed at an imaging spectrometer where elastic scattered photons (same wavelength as the laser source) are first filtered out and inelastic returns are diffracted on a gated intensified-CCD (ICCD). The gated ICCD, in addition of recording the spectral distribution of the inelastic scattered signals, determined the range bin where the measured inelastic scatter originated by adjusting the time delay and the duration of the intensification state of the ICCD camera. Once acquired, the spectra are processed and analyzed by a computer system.

For the case where the averaged concentration of inelastic scatters within the probed volume does not vary too rapidly, the spectra recorded may be the result of several laser pulses binned over a few seconds. This has the advantage of detecting very low signals without the need for a powerful laser providing large pulse energies, an avenue opening the door to mini/micro lasers. The acquired signal, in addition to providing a measure of the concentration of inelastic scatters, can also provide information on their types based on the spectral information contained in that signal. Simard et al. (Ref.4) have demonstrated that two types of biological aerosols (*Bacillius subtilis var globiggi* and *Erwinia herbicola*) aerosolized in open-air have distinct spectral structures. Even if that spectral structure may be in large part dictated by the method of preparation or growth of the bioaerosols, they demonstrated that the detected spectral structure was stable and reproducible for all releases associated with a given batch of biological material.

The short-range BioSpectra concept described above presents schematically the general approach proposed to perform the monitoring of bioaerosol within air volumes located at short-ranges. The limit in sensitivity of such device depends on several parameters. Many of these parameters can be assessed from previous works (as in Ref.4) or by monitoring commercially available technologies (examples are the

10 For the present study, we will assume that the transmitter has a perfect optical design with an optical resolution well below the diameter of the single mode fiber.

power and size of laser sources, the quantum efficiency of ICCDs or the transmission of spectrometers). However, one aspect that cannot be directly determined from the literature or other information sources is the collecting efficiency of a short-range LIDAR transmitter such as the one detailed in Fig.1. This important aspect is analyzed in depth in the following Sections.

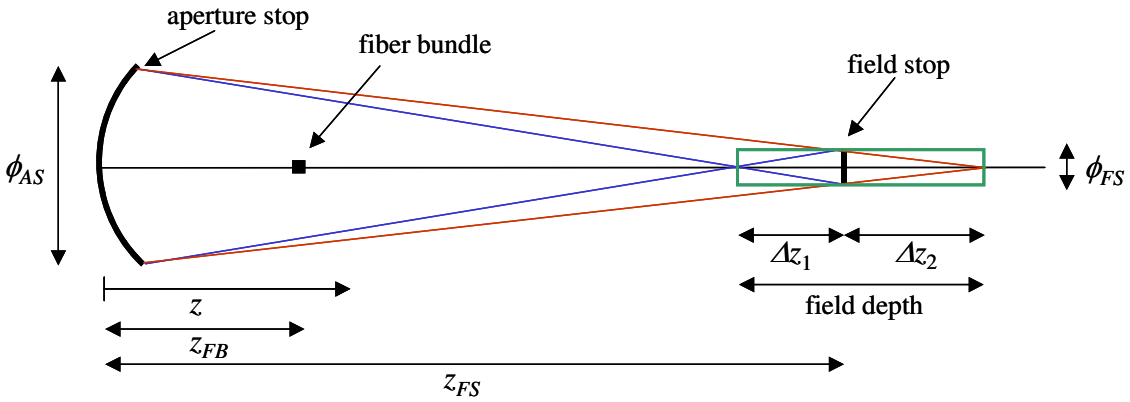

Fig.2 Optical geometry of a co-focal transmitter. The position on the optical axis is given by *z*. A field stop of diameter ϕ_{FS} is formed at position z_{FS} by the image of the fiber bundle (located at z_{FB}) made by the main mirror, that is also the aperture stop of the transmitter with a diameter ϕ_{AS}. This optical design forms a field depth (equals to $\Delta z_1+\Delta z_2$) delimiting the furthest positions on the optical axis relative with the field stop position where all optical rays passing simultaneously through the field stop and the aperture stop reach the fiber bundle.

3.2 Analysis of the geometrical form factor

In Section 2.2, we have shown, within the limits associated with a few approximations acceptable for a short-range LIDAR transmitter, that the spectral energy detected E_λ^i during a period Δt for a scatter *i* located at a range *R* is given by Eqs.11. In this equation, $E_\lambda^i(R,\Delta t,\lambda_0)$ is defined as a product of spectrally dependent or scalar coefficients and an integral $\Phi(R,\Delta t)$ (see Eq.12) taking into account the optical geometry of the probed volume. In order to solve this integral, the optical geometry of the short-range transmitter must be modeled as a function of the spatial dependency of the geometrical form factor ξ.

To model a short-range LIDAR transmitter, several geometric parameters must be defined. Fig.2 described the proposed co-focal transmitter design where these parameters are identified. In this design, z is the distance from the main mirror on the optical axis. A fiber bundle formed of a single mode emitting fiber surrounded by collecting multi-mode fibers is positioned at a distance z_{FB} from the main mirror. This main mirror of diameter ϕ_{AS} and focal length *f,* is the aperture stop of the transmitter. It defines the collecting area. The position of the fiber bundle is chosen to create a conjugate image at a range z_{FS} from the main mirror. The diameter of this conjugate

image ϕ_{FS} defines the field stop of the transmitter. The field stop delimits the incident optical rays directed at the aperture stop that will effectively be collected by the fiber bundle. Fig.2 also depicts the field depth, an important geometric parameter in the resolution of $\Phi(R,\Delta t)$, with a width equals to the sum of Δz_1 and Δz_2. These two range intervals define the furthest positions on the optical axis relative to the field stop where all optical rays passing simultaneously through the field stop and the aperture stop will reach the collecting fiber bundle.

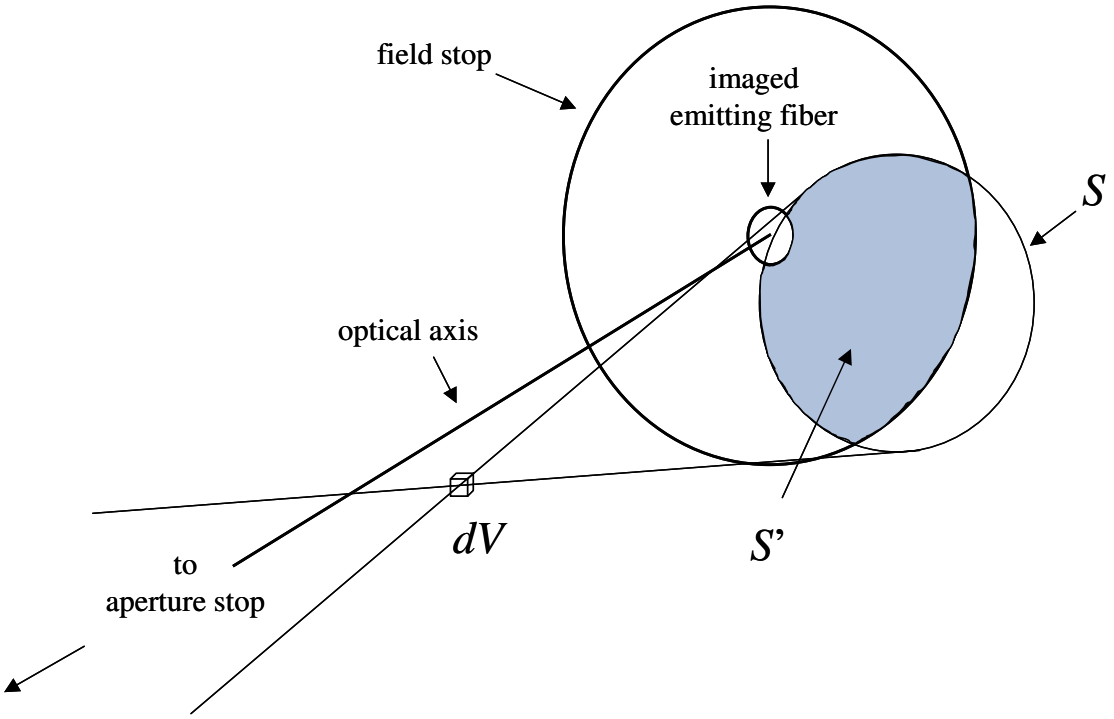

Fig.3 Schematic representation of the geometric form factor ξ for a volume element dV. ξ is defined as the ratio S'/S where S is the base of a cone at the field stop plane formed by all optical rays linking the aperture stop and dV. S' is the fraction of S lying within the field stop area.

With the geometry depicted by Fig.2, the dependency of the ξ in Eq.12 with the position of a volume element dV (dA x dz) can now be characterized. The geometric dependency of ξ can be defined by analyzing the fraction of the total rays linking the aperture stop area and a volume element dV that reaches the field stop (see Fig.3). The envelope of these rays forms two cones connected by their common summit dV. The base of one cone is the aperture stop and the second is the projection field S at the field stop plane. S forms a circle of radius r_{PF} defined as a function of z as

$$r_{PF} = \frac{|z - z_{FS}|}{z} r_{AS}, \tag{13}$$

where r_{AS} is the radius of the aperture stop and z is the position of dV. S' is the part of this area that falls within the field stop. With these definitions, ξ is quantified as the

ratio *S'/S* and could be resolved numerically over the whole volume of integration in Eq.12. However, considering the objective of the present document that is to assess the sensitivity of a short-range LIDAR as a function of its optical design, an analytical model with minimal approximations is introduced. This analytical model has the advantage of describing explicitly the sensitivity as a function of key optical parameters that facilitates the model interpretation. A description of this analytical model is detailed in the next few paragraphs.

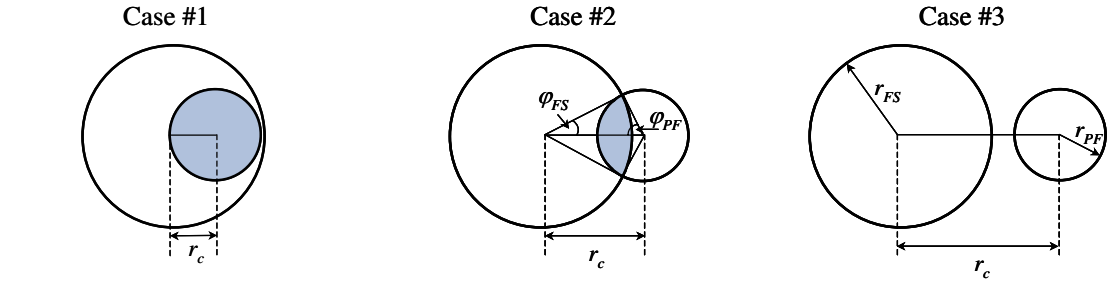

Case #1: $r_c < |r_{FS} - r_{PF}|$

$$\xi(r_c, z) = \begin{cases} 1 & (r_{FS} > r_{PF}) \\ \dfrac{r_{FS}^2}{r_{PF}^2} & (r_{FS} < r_{PF}) \end{cases}$$

Case #2: $|r_{FS} - r_{PF}| < r_c < r_{FS} + r_{PF}$

$$\xi(r_c, z) = \frac{r_{PF}^2 \varphi_{PF} + r_{FS}^2 \varphi_{FS} - r_{FS} r_c \sin\varphi_{FS}}{\pi r_{PF}^2}$$

$$\varphi_{PF} = \cos^{-1}\left[\frac{r_c^2 + r_{PF}^2 - r_{FS}^2}{2 r_{PF} r_c}\right]$$

$$\varphi_{FS} = \cos^{-1}\left[\frac{r_c^2 + r_{FS}^2 - r_{PF}^2}{2 r_{FS} r_c}\right]$$

Case #3: $r_c > r_{FS} + r_{PF}$

$$\xi(r_c, z) = 0$$

Fig.4 Numeric model defining the overlap form factor ξ (see *S'/S* in Fig.3) for the three possible geometries associated with the position of the volume element *dV* in Eq.12. Case #1, the projected field *S* is contained within the field stop (or, mathematically equivalent, the field stop is contained within *S*). Case #2, *S* is partially contained within the field stop and case #3, *S* is outside the field stop. r_{FS} is the radius of the field stop and r_{PF} is the radius of the projected field identified by *S* in Fig.3 and quantified with Eq.13.

The following discussion addresses only the volume of integration in front of the field stop (within Δz_1). However, an equivalent analysis (closely symmetrical) could be developed for the volume behind the field stop (within Δz_2). From the geometrical considerations that have defined ξ as *S'/S* and the cylindrical symmetry of the problem, ξ can be defined as a function of r_c reporting the cylindrical position of *dV*. If we neglect the small volume in front of the image of the emitting fiber where the backscatter signal is not collected (this approximation will be revisited below), a mathematical solution describing ξ as a function of r_c and z can be derived from a simple overlap factor analysis (see Ref.5). The main result of this model is reproduced in Fig.4. In this figure, 3 cases are identified. Case #1 describes the quantity ξ for the situation where the projected field *S* (of radius r_{PF}) is contained within the field stop, or mathematically equivalent, that the field stop is contained within *S*. Case #2

describes the quantity ξ for the cases where part of the projected intensity is within the field stop and case #3 describes the quantity ξ for the situations where the projected intensity is outside the field stop. Based on this model, 3 volumes can be identified. First there is the conical volume where ξ=1 ($r_{FS} > r_{PF}$ and $r_c < r_{FS} - r_{PF}$). This volume is identified in homogeneous grey color in Fig.5. Second, within the same range interval, there is the volume surrounding this cone. In this peripheral volume, ξ varies from 1 to 0 as the distance from the optical axis increases. Fig.6 shows the plot of the dependency of ξ with r_c within these two volumes (left y axis). The third zones is associated with the range interval outside the field depth (z_{FS}-$z>\Delta z_1$) where $r_{PF}> r_{FS}$. Within this zone, ξ varies with r_c from a constant maximum (r_{FS}^2 / r_{PF}^2) inside the cone opposed by the summit (at $z=z_{FS}-\Delta z_1$ and r_c=0) with the first one (identified in dashed grey in Fig.5) to 0 as r_c extends outside this cone at a value greater than $r_{FS} + r_{PF}$. Fig.6 shows this dependency of ξ as a function of r_c (right y axis) in this third zone.

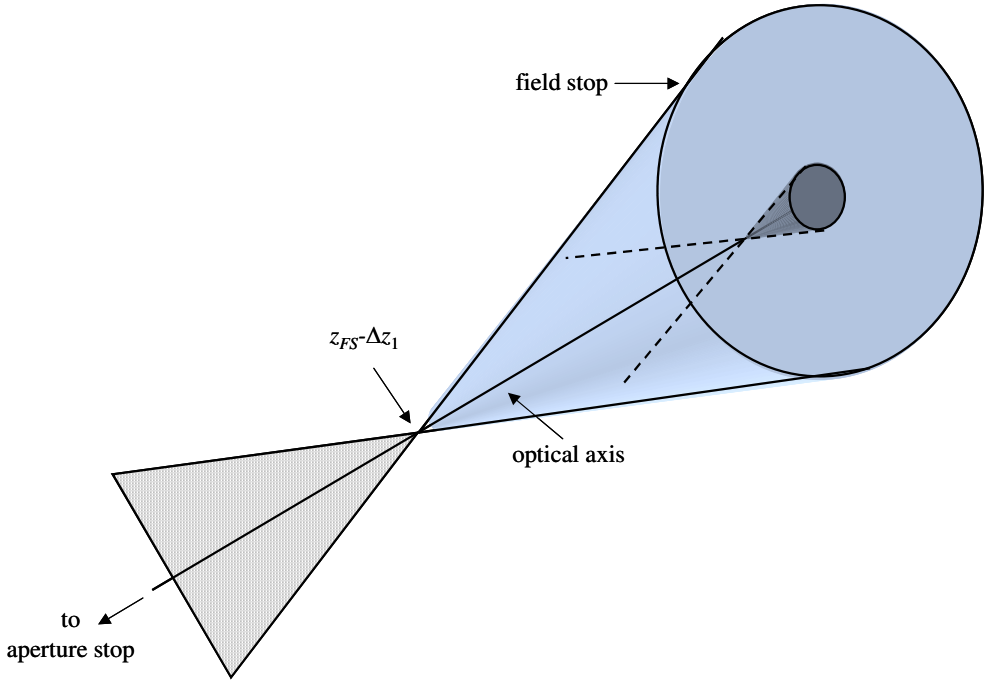

Fig.5 Schema identifying the 3 main volumes in front of the field stop where 3 different variability of ξ are identified. The continuous grey zone corresponds to the volume where ξ is unity. The textured grey region corresponds to the volume where ξ is constant for a given position on the optical axis. The third volume surrounds these grey areas where ξ varies from a constant value to 0 as the distance to the optical axis increases.

From the analysis of the variability of ξ as a function of the position of dV presented in the previous paragraph, two rules can be identified to maximize the integral Φ in Eq.12 and optimize the collecting efficiency of the short-range LIDAR.

First, the range of integration expressed as a function of time as $2R/c$ to $2R/c+\Delta t$ in Eq.12 should be limited around the field depth where ξ is maximized. Integrating outside this range could contribute to increase the collected signal. However, this increased signal comes at a cost of a reduced signal to noise ratio of the measurement when background radiance contributions are significant (see Section 3.5). An optimum limit of integration based on this consideration is to define the range R and the duration of the integration Δt in Eq.12 as

$$R = z_{FS} - \Delta z_1 - c\,\tau_p \quad \text{and} \tag{14}$$

$$\Delta t = 2(c\,\tau_p + \Delta z_1 + \Delta z_2)/c\,. \tag{15}$$

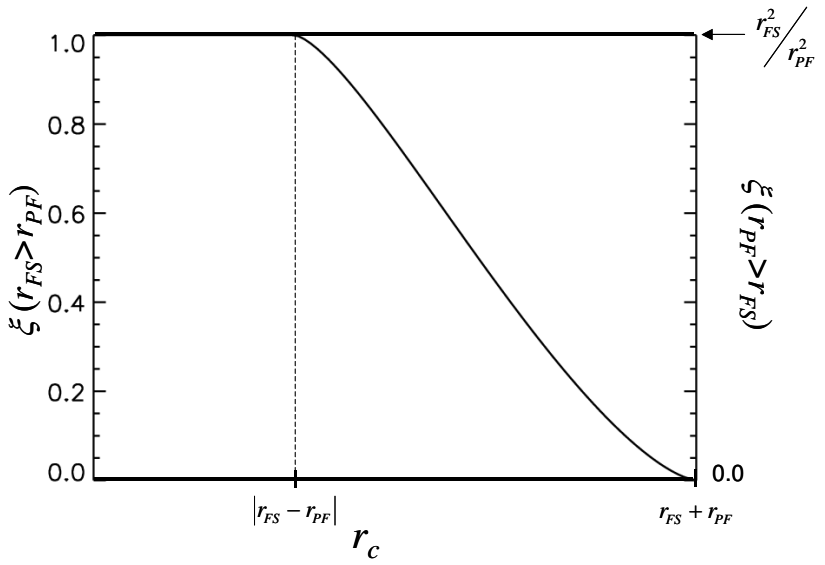

Fig.6 Plot of the overlap function ξ as a function of the distance to the optical axis r_c for the regions depicted in figure 5. Based on the arithmetic model detailed in figure 4, ξ is reported on the left y-axis for the region within the field depth region. Outside the field depth region, ξ is reported on the right y-axis.

This choice has the advantage of limiting the time period where the backscattered signal is detected to the period where the laser pulse enters and exits the field depth region, the region where ξ is maximized. Second, the distribution of the irradiance within the field depth will thus be confined as close as possible to the optical axis region where, once again, ξ is maximized. With these two conditions satisfied, a constant averaged value for the geometrical form factor $\overline{\xi}$ greater than 0.5 could be introduced to approximate the integral Φ in Eq.12. That allows replacing $\xi(z,\vec{r_c})$ in this equation with a constant factor $\overline{\xi}$ and moves it outside the cross-area integral function of $d\mathrm{A}$. This reduces Eq.12 to

$$\Phi(R,\Delta t)=\bar{\xi}\int_{2R/c}^{2R/c+\Delta t}\left[\int_{z=c(t-\tau_f-\tau_p)/2}^{z=ct/2}\frac{1}{z^2}\,dz\right]dt\,. \tag{16}$$

It is interesting to note that this approximation makes the integral Φ independent of the laser intensity across the optical axis.

Once again, the integral in Eq.16 could be completely solved analytically. However, the resulting expression for Φ after the insertion of the expressions for R and Δt from Eqs. 14 and 15 would become algebraically complex to interpret as a function of the transmitter optical design parameters. Since the goal of this report, as stated earlier, is to evaluate the range of sensitivity achievable with a short-range LIDAR, an additional approximation is introduced. The position along the optical axis z in the expression $1/z^2$ of Eq.16 is approximated as constant and the position of the field stop z_{FS} is used. This approximation is valid as long as 1/z <<1 over the range of integration defined by Eq.16. This will be true as long as R, the initial range from where the backscatter signal is detected, does not become too short. Under this condition, after introducing Eqs.14 and 15 in eq. 16, a minimum value for Φ is derived as

$$\Phi(R,\Delta t)=\frac{c\,\bar{\xi}\,\Delta t(\tau_f+\tau_p)}{2\,z_{FS}^2}\,. \tag{17}$$

Finally, by combining the Eqs.11, 15 and 17, the spectral energy detected by a short-range LIDAR is derived as

$$E_\lambda^i(\lambda_0)=\frac{\mathrm{A_{AS}}\,t_\lambda^o\,\Psi_i(\lambda_0)\mathrm{A}_i\,\zeta_\lambda^i(\lambda_0)\mathrm{N}_i\,E_L\bar{\xi}(c\,\tau_p+\Delta z_1+\Delta z_2)}{4\pi\,z_{FS}^2}\,. \tag{18}$$

This last equation will be used in Section 3.4 to evaluate sensitivity of a short-range LIDAR as a function of the optical design of the transmitter.

In Fig.5, a smaller cone shown in black is identified. This region results from the obscuration created by the single mode fiber. Since this fiber does not carry the collected backscatter to the detector, the scatter signal originating from this region and collected by the aperture stop will not be detected. An analysis very similar to the larger cones can be established, this time using the image of the single fiber mode replacing the field stop. Such analysis would show that ξ=0 in the black conical volume and would reach the values previously detailed as the projected field move aside from the image of the single mode fiber at the field stop plane. However, since the diameter of the single mode fiber can be chosen to be less than 1/10th of the fiber bundle, it is anticipated that the effect of this obscuration on $\bar{\xi}$ would be much less than 10 % and will be neglected in the analysis presented by this report.

In order to complete the justifications allowing the introduction of an averaged geometric form factor $\bar{\xi}$ within the volume of integration stated by Eq.12, the spatial

distribution of the laser irradiance within the field depth region must be characterized. This is done in the following Section.

3.3 Analysis of the laser irradiation geometry

In the previous Section, the dependency of the geometrical form factor ξ within the field depth of a short-range LIDAR transmitter has been analyzed. However, to complete the approximated solution of the integral in Eq.12, the spatial distribution of the laser irradiation must also be characterized within that region.

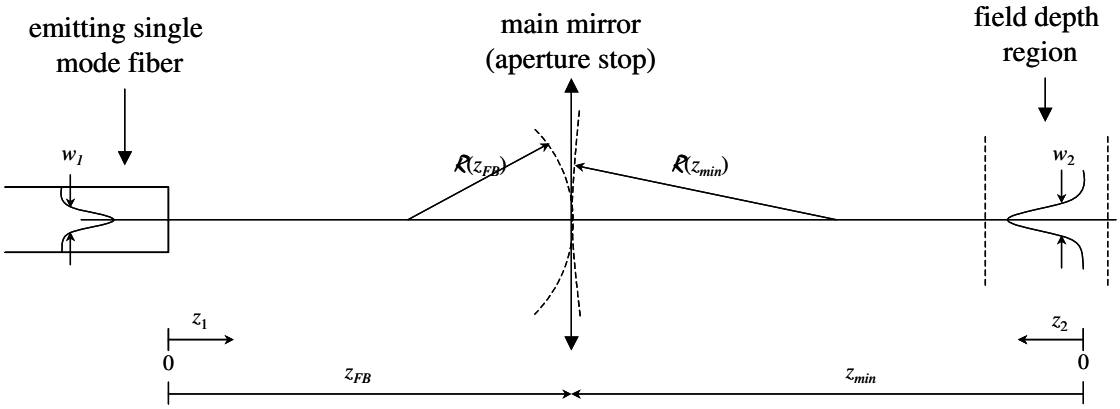

Fig.7 Schematic description of the single mode fiber irradiation geometry. This geometry is based on the model proposed by Kogelnik and Li (Ref.6) describing the cross section of the irradiation as a propagating Gaussian function. This model defines the irradiation in the field depth region of a short-range LIDAR as proposed by the SR-BioSpectra concept (see Fig.1) as a function of the size and position of the emitting single mode fiber and the focal length of the main mirror.

To characterize the laser irradiation within the field depth, the theory of laser beam propagation developed by Kogelnik and Li (Ref.6) is introduced. This formalism is valid either for pulsed or continuous laser sources. This model can also be applied to laser pulses delivered with a single mode optical fiber source as proposed with the SR-BioSpectra concept depicted in Fig.1.

The Kogelnik model derives the waist and field curvature of a laser light beam as a function of the propagation distance. It describes the irradiation in a plane perpendicular to the optical axis as a Gaussian function. However, for the approximated solution proposed in this report, only the waist of the Gaussian beam[11] will be associated with the diameter of the cylindrical area $A_L(z)$ introduced in Section 2.2 as the cross area within the field depth region where an uniform irradiation is proposed (see Eq.12).

Kogelnik and Li have demonstrated that the law dictating the propagation of a Gaussian laser beam can be completely described with two interrelated equations. The

11 The waist of a Gaussian light beam is defined as the diameter where the intensity is at $1/e^2$ times its maximum.

first equation defined the beam radius w (at $1/e^2$ in intensity) as a function of the propagation distance z_i as[12]

$$w^2(z_i) = w_0^2\left[1+\left(\frac{\lambda z_i}{\pi w_0^2}\right)^2\right] \tag{19}$$

and the second equation describes the radius of curvature $\mathcal{R}$ of the beam wave front as a function of the propagating distance as

$$\mathcal{R}(z_i) = z_i\left[1+\left(\frac{\pi w_0^2}{\lambda z_i}\right)^2\right]. \tag{20}$$

In these two equations, λ is the laser wavelength and w_0 is the beam minimum radius located at $z_i = 0$. Applying this model to the short-range LIDAR geometry pictured in Fig.2 requires resolving the set of Eqs. 19 and 20 between the fiber bundle and the main mirror (the aperture stop), and between the main mirror and the field stop. Solving the condition limits at the fiber bundle and aperture stop planes will provide a complete solution for $A_L(z)$ in the field depth region. Fig.7 shows schematically the geometric parameters defining the laser irradiation within these two regions. In this figure, z_1 and z_2 identified the position along the optical axis in the region between the emitting fiber and the aperture stop (object side), and between the field depth region and the main mirror (image side), respectively. z_{min} is the distance from the main mirror where the minimum beam waist is located on the image side. It is important to note that the position where the minimum beam waist is located on the image side is not equivalent to z_{FS} (see Fig.2). This results from the infinite radius of curvature of the irradiation amplitude at the output face of the emitting single mode fiber (location of minimum beam waist on the object side). However, this difference between z_{min} and z_{FS} is minimized as the size of the beam waist at the output fiber approaches the dimension of the wavelength. Since the single mode emitting fiber has a size comparable to the wavelength, negligible effects are anticipated from the displacement between the minimum beam waist and the field stop with the proposed model for most optical designs.

In Chapter 4, the Eqs.19, 20 and the considerations detailed in the previous sections will be used to quantify the eq.18 as a function of different optical parameters defining the transmitter design. To complete this quantification and obtain a prediction in sensitivity for a given short-range LIDAR optical design, the basic fluorescence parameters of the inelastic scatters found in Eq.18 must be assessed. These will be deduced from the results obtained from previous trials performed with a long-range inelastic LIDAR: the SINBAHD system. These considerations are detailed in the following section.

---

12 The indexed position along the optical axis z_i is introduced to emphasize the different positions of the origin depending on whether the object or the image region is analysed (see fig.7).

3.4 Quantifying the sensitivity of a short-range inelastic LIDAR to detect bioaerosol by comparison with the SINBAHD results

In order to interpret quantitatively the model developed in the previous sections and to obtain sensitivity predictions, the standard deviation associated with the noise floor of a spectrometric LIDAR $\langle E_f \rangle$ is introduced. This is the detected signal integrated over the spectra when no fluorescence is generated within the probed volume. This quantity is the combined result of the noise generated by the background radiance and the contribution of electronic noise (see Section 3.5). To relate this noise floor with a sensitivity to detect a given concentration of inelastic scatter, Eq.18 is first integrated over the spectra as

$$E_i = \int_\lambda E_\lambda^i \, d\lambda = \frac{\mathrm{A_{AS}} \ \Psi_i \, \mathrm{A}_i \, \mathrm{N}_i \, E_L \bar{\xi} (c\tau_p + \Delta z_1 + \Delta z_2)}{4\pi \, z_{FS}^2} \int_\lambda t_\lambda^o \, \zeta_\lambda^i \, d\lambda \ . \tag{21}$$

Then, for simplification, the integral and some of the parameters that depend only on the scatter properties are combined within a single factor Γ_i. With this new formulation, the standard deviation of the collected signal $\langle E_i \rangle$ is related to an error in the measurement of scatter concentration $\langle \mathrm{N}_i \rangle$ as

$$\langle E_i \rangle = \Gamma_i \frac{\mathrm{A_{AS}} \ E_L \, \bar{\xi} \ (c\tau_p + \Delta z_1 + \Delta z_2)}{z_{FS}^2} \langle \mathrm{N}_i \rangle . \tag{22}$$

By replacing $\langle E_i \rangle$ by $\langle E_f \rangle$ in this last equation, the noise floor of a given LIDAR can be expressed as a standard deviation in concentration of scatter *i* as

$$\langle \mathrm{N}_i \rangle_f = \frac{z_{FS}^2}{\mathrm{A_{AS}} \ E_L \, \bar{\xi} \ (c\tau_p + \Delta z_1 + \Delta z_2) \ \Gamma_i} \langle E_f \rangle . \tag{23}$$

This last equation is useful to compare the sensitivities anticipated with different LIDAR designs.

In the present report, the results reported by Simard (Ref.1) are introduced as a reference to quantify the scatter dependent parameters. From this report, an equation very similar to Eq.23 can be derived as

$$\langle \mathrm{N}_i^S \rangle_f = \frac{r_S^2}{\mathrm{A}_{AS}^S \ E_L^S \, \bar{\xi}_S \ \Delta r_S \ \Gamma_i^S} \langle E_f^S \rangle \tag{24}$$

where r_S is the range to the probe cell and the index *S* identifies the parameters associated with the SINBAHD device, a spectrometric inelastic LIDAR designed for long-range biodetection and extensively tested with bioaerosol simulants. By dividing

Eq.23 (where we inserted the index *SR* to identified the short-range LIDAR parameters) by Eq.24, the following result is derived,

$$\left\langle \mathrm{N}_i^{SR} \right\rangle_f = \frac{\mathrm{A}_{AS}^{S}\ E_L^S\ \overline{\xi_S}\ \Delta r_S\ z_{FS}^2}{\mathrm{A}_{AS}^{SR}\ E_L^{SR}\ \overline{\xi_{SR}}\ (c\tau_p + \Delta z_1 + \Delta z_2)\, r_S^2} \frac{\Gamma_i^S}{\Gamma_i^{SR}} \frac{\left\langle E_f^{SR} \right\rangle}{\left\langle E_f^S \right\rangle} \left\langle N_i^S \right\rangle_f . \tag{25}$$

At night, it has been observed that the noise floor is essentially the result of the electronic noise contribution (see Section 3.5). Since it is reasonable to assume that the noise floor of the electronics of detection for a short-range LIDAR will be as good if not better than the one used by the SINBAHD system, the ratio of noise floors at night in Eq.25 can be approximated as one. Similar arguments can be advanced for the spectral transmission of the transmitter which should not be a parameters presenting large variations between a long-range LIDAR like SINBAHD and a short-range LIDAR as the SR-BioSpectra. This implies that the ratio of Γ in Eq.25 combining the spectral transmission of the transmitter and the scatter dependent parameters can also be approximated as one.

Table 1 Parameters associated with the SINBAHD long-range spectrometric LIDAR for a single measure.

Laser energy delivered (E_L^S)	190 J
Geometrical form factor ($\overline{\xi_S}$)	0.88
Area of aperture stop (A_{AS}^S)	0.073 m^2
Integrated range interval (Δr_S)	5 m
Range of detection (r_S)	1388 m

With the parameters of the SINBAHD device reported by Simard (Ref.1) and reproduced in Table 1, a noise floor sensitivity at night $\left\langle N_{BG}^S \right\rangle_f^N$ of about 5 ACPLA (Agent Contained Particle per Liter of Air) for the bioaerosol simulant *Bacillius subtilis var globiggi* (or BG) is obtained. With these parameters and the simplifications mentioned above, Eq.25 is reduced to

$$\left\langle \mathrm{N}_{BG}^{SR} \right\rangle_f^N = \frac{z_{FS}^2}{\mathrm{A}_{AS}^{SR}\ E_L^{SR}\ \overline{\xi_{SR}}\ (c\tau_p + \Delta z_1 + \Delta z_2)} \times (3.2 \times 10^{-5}\ \mathrm{J \cdot m}) \times 5\ \text{ ACPLA.} \tag{26}$$

In Chapter 4, this last equation will be used to predict the sensitivity (in ACPLA of BG) of a short-range inelastic LIDAR as a function of its optical design parameters (essentially the size of the collecting aperture and the range of detection).

3.5 Modeling the background parasitic signal dictating the sensitivity of a short-range spectrometric LIDAR

In the previous Section, introducing the results from the SINBAHD project has allowed quantifying the sensitivity of a short-range spectrometric LIDAR to detect bioaerosol as a function of the design parameters. This model was based on the noise floor obtained at night where it is dominated by the contribution from the electronics of detection. To anticipate this noise floor when the background radiance is not negligible[13], the model used in the previous Section must be modified.

Simard (Ref.1) proposed a shot noise statistic to describe the noise floor of the SINBAHD system and quantified it as

$$\langle E \rangle_f = \sqrt{2 \times E_b + \Delta}\,, \tag{27}$$

where E_b is the total number of photons originating from the background radiance (and detected simultaneously with the laser induced inelastic backscattered signal) and Δ is the equivalent number of photons that would correspond to the noise floor of a measurement resulting only from the electronics of detection. Note that the factor 2 is introduced to take into account the two measurements that must be acquired to correct the laser induced signal from the background radiance contribution[14]. The background radiance contribution can be derived as

$$E_b = \int_\lambda E_\lambda^b d\lambda = \mathrm{A}_{AS}\, \Omega\, n\, \tau_g \int_\lambda t_\lambda^o \Pi_\lambda d\lambda\,, \tag{28}$$

where Ω is the solid angle corresponding to the field of view of the transmitter, τ_g is the time period (or gate) used to collect the signal resulting from one pulse laser, n is the number of laser pulse fired at the probed volume to obtain the resulting signal and Π_λ is the natural spectral radiance within the field of view of the transmitter.

In a previous Section, an appreciation of Δ was introduced as an equivalent sensitivity of 5 ACPLA from the results obtained with the SINBAHD system under the specific conditions of acquisition detailed in Table 1. By combining Eqs.23, 27 and 28 under the condition of strong background contribution ($2E_b >> \Delta$), the ratio of noise floor sensitivity between day and night for a given LIDAR system and scatter i can be derived as

$$\frac{\langle N_i \rangle_f^D}{\langle N_i \rangle_f^N} = \frac{\langle E_i \rangle_f^D}{\langle E_i \rangle_f^N} = \sqrt{\frac{2\mathrm{A}_{\mathrm{AS}}\Omega\, n\, \Delta t \int t_\lambda^o \Pi_\lambda d\lambda}{\Delta}}\,. \tag{29}$$

This result shows that this ratio is independent of the scatter i and most of the LIDAR parameters (especially the range) but will be affected (beside the level of background

13 This background radiance could be the result of natural or manmade light sources.

14 In the SINBAHD prototype, this was done by sampling the signal between each laser pulses fired at the probed atmospheric cell with the same conditions of acquisition.

radiance) by the size of the aperture stop A_{AS}, the field of view of the transmitter Ω and the total time of acquisition $n\Delta t$ needed to obtain a measure.

Simard (Ref.1), with the SINBAHD system, has reported a noise floor during sunny day about three times the one obtained at night. Without anticipating precisely the noise floor ratio between day and night, it is important to identify how a variation of the parameters in Eq.29 will affect this ratio of 3 observed with the SINBAHD system for the design of SR-BioSpectra.

4. Quantitative sensitivity predictions of a short-range LIDAR as a function of its optical design

In Chapter 3, the main considerations necessary to predict the sensitivity of a short-range spectrometric LIDAR to detect a bioaerosol cloud of a concentration given in ACPLA have been derived. In the present Chapter, this predicted sensitivity is analyzed as a function of two main variables: the size of the aperture stop A_{AS} and the range of detection defined by the position of the field stop z_{FS}.

Eq.26 reports the sensitivity as a function of the different optical parameters of a short-range LIDAR in concentration of BG as a bioaerosol scatter. This is adequate assuming a similar optical transmission between the short-range LIDAR design and the SINBAHD system. The parameters other than A_{AS} and z_{FS} in this equation can be fixed to quantities representative of the present state of the technology. These representative quantities are listed in Table 2.

Table 2 Representative quantities assigned to selected parameters defining the optical design of a short-range spectrometric LIDAR.

Laser power, P_L	10 mW
Pulse repetition rate, f_L	1000 Hz
Laser pulse duration, τ_p	10 ns
Number of pulse sent for a measurement, n_p[15]	10000
Diameter of the fiber bundle, ϕ_{FB}	50 μm
Diameter of the single mode fiber, ϕ_{SM}[16]	5 μm
Collection field of view, Ω	300 μrad
Averaged geometrical form factor, $\overline{\xi_{SR}}$	0.7
Collecting optic diameter, ϕ_{AS}	5, 10, 15 and 20 cm

Based on Fig.2, several equations can be derived from geometric optical principles to derive the different parameters in Eq.26. These are:

$$z_{FB} = \frac{\phi_{FB}}{\Omega}, \tag{30}$$

$$f = \frac{z_{FB}\, z_{FS}}{z_{FB} + z_{FS}}, \tag{31}$$

$$\phi_{FS} = \Omega \times z_{FS}, \tag{32}$$

15 The number of laser pulses is chosen to obtain a measurement after 10 seconds of binned acquisitions

16 For the present discussion, this dimension is also associated with the diameter of the single mode field at $1/e^2$.

$$\Delta z_1 = \frac{\phi_{FS}}{\phi_{AS} + \phi_{FS}} z_{FS}\,, \tag{33}$$

$$\Delta z_2 = \frac{\phi_{FS}}{\phi_{AS} - \phi_{FS}} z_{FS}\,. \tag{34}$$

Combining Eqs.30-34 with the parameters in table 2 completely defines the sensitivity given by Eq.26 as a function of ϕ_{AS} and z_{FS}. Fig.8 (left) shows a plot of this relation for selected ranges and collection apertures.

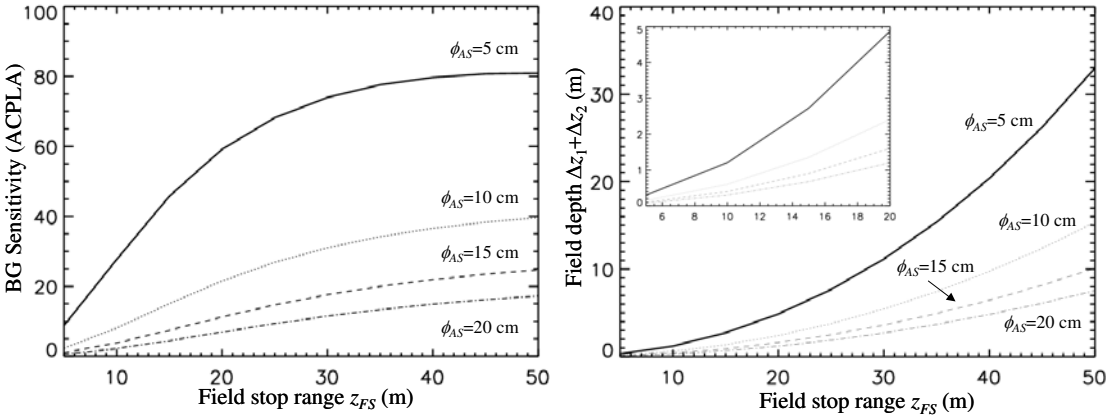

Fig.8 Sensitivity and dimension of the field depth of a transmitter as a function of the range to the field stop and for an aperture stop diameter of 5, 10, 15 and 20 cm. The predicted sensitivity is expressed in concentration of BG measured in ACPLA. The smaller plot embedded in the right plot reports the size of the field depth at short-ranges.

In this figure, the predicted noise floor sensitivity $\left\langle \mathrm{N}_{BG}^{SR} \right\rangle_f^N$ expressed in ACPLA of BG without background parasitic radiance and based on the design parameters listed in table 2 varies from a fraction of one ACPLA to about 80 ACPLA for aperture stop diameter varying from 5 to 20 cm and for field stop position varying from 5 to 50 meters. It is important to note the asymptotic behavior of the noise floor as the field stop position increases. This results from the increases of the field depth ($\Delta z_1+\Delta z_2$) as the range to the field stop z_{FS} is positioned further away from the transmitter. Combining Eqs.32, 33 and 34 shows a dependency of ($\Delta z_1+\Delta z_2$) with the square of z_{FS}[17]. This square dependency contributes to cancelling the relation of $\left\langle \mathrm{N}_{BG}^{SR} \right\rangle_f^N$ with z_{FS} in Eq.26 as the field depth become large in comparison with the laser pulse duration ($\Delta z_1+\Delta z_2 >> c\,\tau_p$). This confers to the short-range LIDAR concept based on conjugated planes[18] a characteristic similar to passive sensors: a sensitivity independent of the range to the targeted cloud as long as the concentration is

17 As long as $\phi_{AS}^2 >> \phi_{FS}^2$.

18 The probed cell is centered on the field stop positioned at the image plane of the fiber bundle, these two planes are optically conjugated by the imaging main mirror.

expressed as the average over the field depth region. This is equivalent to expressing the sensitivity as the product between the averaged concentration of bioaerosol over the field depth times the range interval of this field depth; a quantity referred to as CL for passive sensors. Based on this consideration, it is important to relate the sensitivity provided by Fig.8 with the corresponding range interval of the field depth.

Fig.8 (right plot) shows how the field depth enlarges as the field stop range increases. The embedded plot shows this quantity at short ranges. From these results, it is anticipated that the range interval where fluorescent aerosols are probed with corresponding sensitivity becomes an important fraction of the total range as the range to the field stop increases (especially for a small aperture stop). As discussed in the previous paragraph, the sensitivity detailed in Fig.8 (left plot) corresponds to an averaged concentration of BG over the corresponding total range interval. If a shorter range interval within the field stop is desired for a given application, the sensitivity reported by Fig.8 (left plot) would degrade following Eq.26 where $\Delta z_1+\Delta z_2$ is replaced by the range interval of interest (ideally centered at the position of the field stop).

A representative value of 0.7 for $\overline{\xi_{SR}}$ is proposed in table 2. This is anticipated from the discussion in Section 3.2 on the geometry of collection and is based on the assumption of a laser beam irradiation close to the optical axis within the field depth region. Therefore, it is important to verify the geometry of the irradiation laser beam within the field stop region. This is done by combining the optical parameters defined by Eqs.30-34 with the Gaussian irradiation model described by Eqs.19, 20 and Fig.7. From this combination, 6 equations are formulated to describe the irradiation geometry within the field depth region. These equations are:

$$w_1^2(z_{FB}) = w_1^2\left[1+\left(\frac{\lambda z_{FB}}{\pi w_1^2}\right)^2\right] \quad \Rightarrow \begin{cases} z_{FB} \text{ known} \\ w_1 \text{ known} \\ w_1(z_{FB}) \text{ derived} \end{cases} \tag{35}$$

$$\mathcal{R}_1(z_{FB}) = z_{FB}\left[1+\left(\frac{\pi w_1^2}{\lambda z_{FB}}\right)^2\right] \quad \Rightarrow \{\mathcal{R}_1(z_{FB}) \text{ derived} \tag{36}$$

$$w_2(z_{min}) = w_1(z_{FB}) \quad \Rightarrow \{w_2(z_{min}) \text{ derived} \tag{37}$$

$$\frac{1}{\mathcal{R}_2(z_{min})} = \frac{1}{\mathcal{R}_1(z_{FB})} - \frac{1}{f} \quad \Rightarrow \begin{cases} f \text{ known} \\ \mathcal{R}_2(z_{FB}) \text{ derived} \end{cases} \tag{38}$$

$$w_2^2(z_{min}) = w_2^2\left[1+\left(\frac{\lambda z_{min}}{\pi w_2^2}\right)^2\right] \quad \Rightarrow \begin{cases} z_{min} \text{ unknown} \\ w_2 \text{ unknown} \end{cases} \tag{39}$$

$$\mathcal{R}_2(z_{min}) = z_{min}\left[1+\left(\frac{\pi w_2^2}{\lambda z_{min}}\right)^2\right] \quad \Rightarrow \begin{cases} z_{min} \text{ unknown} \\ w_2 \text{ unknown} \end{cases} \tag{40}$$

In this set, the derived parameters are detailed at the right of each equation. Eqs.37 and 38 are derived by applying thin lens optical laws at the aperture stop thus dictating the conservation of the beam diameter and the change of field curvature produced by the main mirror. Eqs.39-40 must be uncoupled to derive the position z_{min} and the radius w_2 of the minimum beam waist within the field depth region. After simple algebraic manipulations, these 2 equations are uncoupled as

$$z_{min} = \frac{\mathcal{R}_2(z_{min})}{\left(\lambda \mathcal{R}_2(z_{min})/\pi w_2^2(z_{min})\right)^2 + 1} \quad \Rightarrow \{z_{min} \text{ derived} \tag{41}$$

$$w_2 = \frac{w_2(z_{min})}{\sqrt{\left(\pi w_2^2(z_{min})/\lambda \mathcal{R}_2(z_{min})\right)^2 + 1}} \quad \Rightarrow \{w_2 \text{ derived} \tag{42}$$

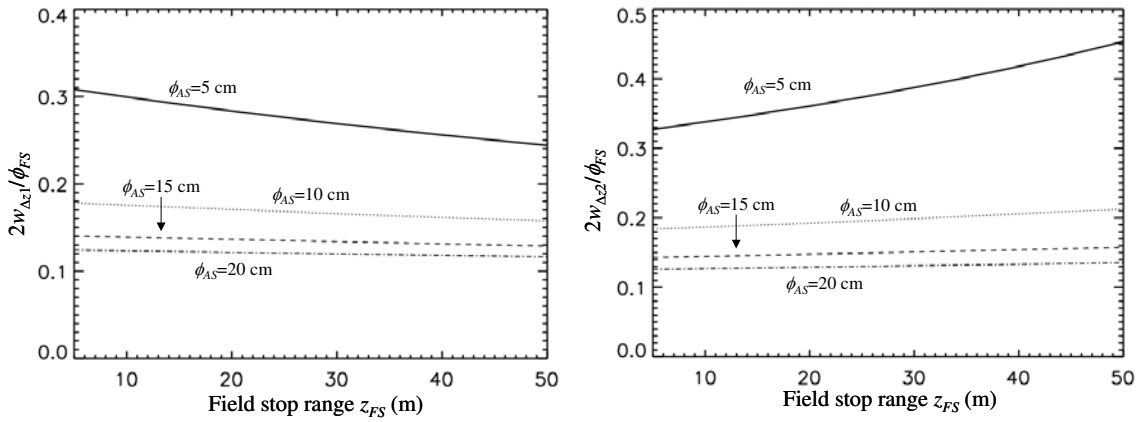

Fig.9 Plots of the ratios between the laser irradiation and the field stop diameters at the entrance (left plot) and exit (right plot) points of the field depth region as a function of the range to the field stop and for aperture diameters of 5, 10, 15 and 20 cm.

Once inserted in Eqs.19 and 20, this last set of equations provides the two main parameters completely defining the irradiation geometry fired along the optical axis by the transmitter. This allows comparing the ratio of the diameters between the irradiation beam at the limits of the field depth regions (z_{FS}-Δz_1 and z_{FS}+Δz_2) with the one of the field stop. Figs.10 and 11 show these ratios for four diameters of aperture stop and ranges to field stops varying from 5 to 50 meters. A first observation, if we ignore the results for the 5 cm aperture stop, is that this ratio is about 0.2 or less for all investigated geometric designs. These results support well the value of 0.7 proposed for the geometric form factor averaged over the field depth region. The increased ratios obtained with the 5 cm aperture stop result from the longer field depth relative to the range to the field stop associated with the small aperture stop transmitter design. On the other hand, the reduction of this ratio at the shorter end of the field depth

region (Fig.9, left plot) and its increase at the further end (Fig.10, right plot) as the range to the field stop extends, results mainly from the differences in position between the minimum irradiation beam waist and the field stop. This difference is shown in Fig.10 (left plot) as a function of the range to the field stop (note that the minimum beam waist occurs within the closer half of the field stop region).

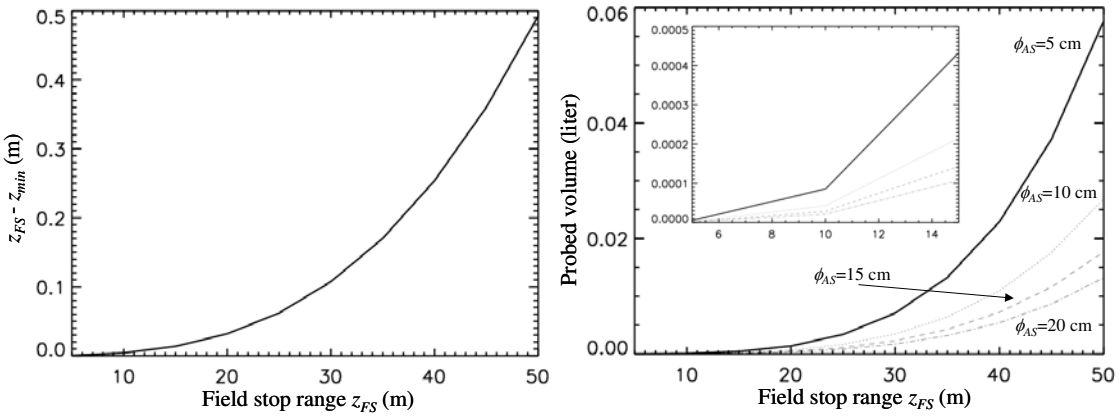

Fig.10 Difference in position between the field stop and the minimum laser irradiation beam waist as a function of the position of the field stop (left plot) and the size of the volume probed by the short-range LIDAR (right plot) as a function of field stop position and aperture stop diameters of 5, 10, 15 and 20 cm. The smaller embedded plot shows a magnification of the probed volume at short-range.

Two other aspects associated with the design of a short-range LIDAR for bioaerosol detection deserve to be investigated: the probed volume and the numerical aperture of the transmitter. The volume crossed by the laser beam within the integrated range interval defines the probed volume. It defines the number of scatters, for a given concentration, that contribute to the signal returned to the transmitter. Fig.10 (right plot) shows this volume in liters as a function of the diameter of the aperture stop and the range to the field stop. It is derived as the averaged irradiation beam cross section (evaluated at the minimum and the two extremities of the field depth) times the integrated range interval $c\tau_p+\Delta z_1+\Delta z_2$. By multiplying this volume by the typical sensitivities shows in Fig.8[19], it is easy to deduce that not all fired laser pulses will hit a bioaerosol within the probed volume. Furthermore, when considering ranges below 10 meters and the number of pulses fired for a measurement (n_p=10000, see table 2), there is a non-negligible probability that not a single scatter will be caused by the laser radiation within the probed range interval. Thus there could be no fluorescence produced for a given measure when the bioaerosol concentration approaches the sensitivity limit. This consideration should be taken into account not only in the design of the transmitter but also within the electronics of detection. This issue will be revisited in the discussion.

Finally, Fig.11 shows the numerical aperture (NA) of the transmitter defined as $\sin(\phi_{AS}/2f)$. This dictates the cone of acceptance of the collecting fibers forming

19 A bioaerosol concentration in ACPLA can be defined as the number of active bioaerosol per liter of air.

the fiber bundle. Standard fibers have a NA around 0.2. However, special fibers (that may not be compatible with fiber bundle technology) can be designed with NA greater than 0.5. The latter may be required for short-range LIDAR designs based on the parameters of table 2 and having collecting aperture stops greater than 5 cm. Another possible measure to avoid a large NA is to increase the focal length of the transmitter at the expense of device compactness.

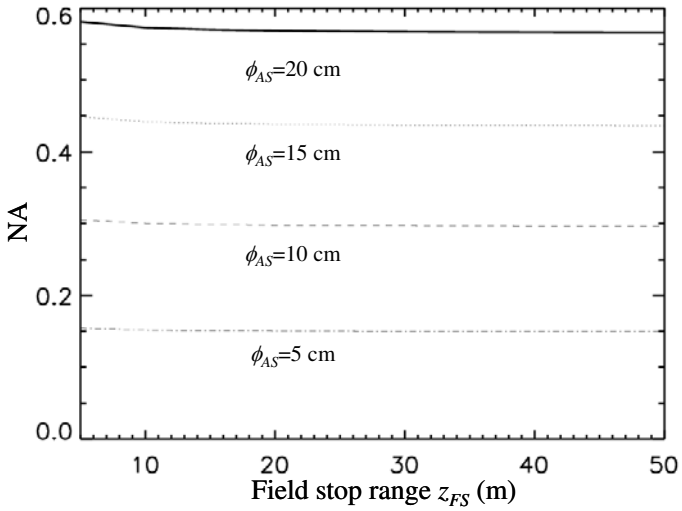

Fig.11 Transmitter numerical aperture as a function of the range to the field stop and for aperture stop of 5, 10, 15 and 20 cm in diameter.

5. Discussion

In the previous Sections, a working model was developed to predict the sensitivity of a short-range spectrometric LIDAR for the detection of bioaerosols by laser induced fluorescence. Specific quantitative projections were detailed for a bioaerosol (*Bacillius subtilis var globiggi* (BG)) based on calibrated measurements made by the SINBAHD project (Ref.1). The derivation of this model has necessitated several approximations. Many aspects associated with this technological approach should be discussed further. Even if these aspects are not directly addressed with the proposed model, they have a direct impact on the capacity of the proposed device to perform efficiently as a short-range standoff biodetector. In the following, the practical consequences of some of these approximations will be revisited and additional considerations that may have an important impact on the capabilities of such an instrument will be briefly discussed.

The significance of the proposed model approximations on the LIDAR predicted sensitivities

Several approximations have been introduced in the model proposed in this report and supporting the bioaerosol cloud sensitivity reported in Chapter 4. The impacts of some of these approximations should have limited impacts on the resulting predictions in sensitivity. This is the case for the assertions made on the fundamental properties of the bioaerosol cross section (Eq.4) obtained by assuming an isometric scattering property (equal probability that a fluorescing photon being emitted in all directions) and an uncorrelated product of parameters (the quantum yield, the spectral signature and the projected area are mutually independent in expressing the quantum yield of a fluorescing aerosol). The anticipated reduced impacts of these fundamental approximations result from the direct introduction of the scatter properties with the experimental measurements obtained in situ with previous works (as the SINBAHD project).

Other approximations that should have limited impacts on the predicted sensitivity are the uniform laser irradiation (instead of Gaussian, Section 2.2) and the averaging of the geometric overlap factor over the field stop (Section 3.2). Since the cross section of the laser beam is small in comparison with the variation in concentration of a bioaerosol cloud (even at ranges of tens of meters), little inhomogeneous effect will result from the uniform irradiation approximation. To quantify, up to a 10 % error in sensitivity originating from the averaged geometric overlap factor approximation is anticipated in the worst cases. This limited deterioration results in part from the fiber bundle approach that confers a natural optical alignment between the emission and the collection optical axes, confining the irradiation volume close to the transmitter optical axis where the geometric overlap factor is maximized. However, at short-range where the field depth becomes comparable to the length of the laser pulse, an important fraction of the collected

scatter may lie outside the field depth region where the geometrical form factor degrades rapidly as a function of the distance to the field stop region. Furthermore, under short-range conditions, the squared short laser pulse and fluorescence time decay approximations (Sec. 2.2) may introduce important variations in the anticipated sensitivity presented in Chapter 4. Part of this deviation will become important as the equivalent length corresponding to the fluorescence decay times the speed of light becomes comparable with the sum of the length of the laser pulse and the field depth region. Such a situation would be equivalent to opening the gated sensor over a short period such that a large part of the induced fluorescence within the field depth region would not have the time to reach the sensor. Notwithstanding this important phenomenon, most fluorescence decay times of bioaerosols are less than or in the order of 5 nsec (~0.75 m), which is comparable with the short laser pulse length used for LIDAR applications. This will contribute to minimizing the effect of the delayed fluorescence even at ranges approaching 5 meters where the field depth region may become less than a half-meter.

Another important approximation that will have important impacts at short-range is the substitution of the position z in the integral detailed by Eq.16 by a constant parameter, the position of the field stop. Even if the field stop is about at the middle position of the integrated range interval, the heavier weight of the $1/z^2$ parameter within the first half of the integrated interval (closer range side) in comparison with the one over the second half (further range side) will contribute to underestimate the sensitivity reported.

One final important aspect to keep in mind when interpreting the anticipated sensitivity depicted by Fig.8 is the assumption of an equivalent spectral transmission between the SINBAHD system and the short-range spectrometric LIDAR under analysis. If this is not the case, this variation should be taken into account in the ratio of factor Γ in Eq.25.

Background parasitic radiance

Based on the principles detailed in Section 3.5, the parasitic background signal dictating the sensitivity of a short-range spectrometric LIDAR can originate from internal electronic noise (usually observed at night) or from the background radiance contribution (day time scenario). This parasitic background signal generating the limiting noise floor of the instrument has been modeled with Eq.27. Under negligible background radiance, this noise floor is essentially dictated by the electronics of detector and, to a certain extent, by the algorithm used to detect the photonic signals (see the following paragraph where the photonic detection pre-processing strategy is described). In the cases where the background radiance is the main contributor to the noise floor, Eq.29 has established a fixed degradation of the sensitivity in comparison to nighttime operations (where electronic noise dominates). This model models the dependence of sensitivity during day time conditions as a function of the square root of the product of four main parameters: the area of the aperture stop, the field of view of the transmitter, the total collection time and the

level of ambient radiance within the spectral interval of collection. For conditions of acquisition similar to the SINBAHD device, a ratio of three for daytime versus nighttime degradation been anticipated for this quantity.

For the design of a short-range LIDAR, a ratio of degradation of 3 in sensitivity between day and night may be challenging to reach. It is true that the smaller aperture stop will contribute to reducing this ratio. However, the high repetition rate (and low peak power) associated with efficient small laser sources and the increase in size of the gated interval (see Fig.8) may contribute to increase in a significant manner the total time of integration corresponding to a single measure.

On the other hand, some scenarios of interest for short-range bioaerosol detection system may involve sites like arenas, stadiums or other semi-enclosed structures. The anticipated lower level of ambient radiance within these sites in comparison with the direct sunny condition under which the SINBAHD system derived its day time noise floor (upon which the Biospectra daytime noise floor estimate is based) will help to achieve a low ratio of sensitivity degradation.

If the ambient radiance of a specific scenario is sufficiently high to generate non-desirable poor sensitivity, a last resort is to reduce the field of view of the transmitter. But, this approach might be rapidly limited by the fiber bundle technology (there are physical limitations dictating the minimum size of a fiber bundle), the transmitter efficiency (reducing the diameter of the fiber bundle will also reduce the field depth and equivalently, the number of scatters contributing to the signal of interest) and the maximum focal length of the transmitter necessary to preserve the compactness characteristics of the short-range LIDAR design.

The parasitic fluorescence contribution

In this document, there is a paramount issue for the design of sensitive inelastic LIDARs that has not been discussed up to here. This issue is the contribution of parasitic induced fluorescence within the spectral interval of transmission of the transmitter and collected simultaneously with the one originating from the fluorescing aerosols of interest. The degradation caused by this parasitic induced fluorescence can be modeled as if it were additional background parasitic radiance. Two scenarios where this occurs can be identified.

First, there is the case where parasitic fluorescence is generated within the emitting fiber and a non-negligible fraction of this fluorescence is coupled directly to the collecting fibers by evanescent mode transfer and is ultimately detected by the gated electronics[20]. It is anticipated this situation may occur at short-range where the fiber fluorescence decay time is comparable with the back and forth transit time of the laser pulse fired by the transmitter at the field depth region and the fluorescence returned to the detector.

20 Here, we identified the fluorescence induced within the emitting fiber as the source of the parasitic contribution. However, fluorescence induced with other optical components of the LIDAR and coupled back into the collecting fibers will produce similar sensitivity degradation.

Second, there is the worst scenario where a fraction of the parasitic fluorescence induced within the emitting fiber stays confined in that fiber to become couple dynamically (with some short delay) with the UV laser pulses fired at the probed cell. This second scenario is very important to avoid because its effect will not depend on the range to the probe cell. Furthermore, the aerosols within the probe cell will elastically return this parasitic fluorescence very efficiently[21] in comparison with the bioaerosol induced fluorescence. Although this source of parasitic radiation can be extremely damaging, it is expected that the fraction of the parasitic fluorescence coupled back into the emitting single mode fiber should be extremely small because of the wavelength cutoff associated with well design single mode fiber. To avoid these phenomena, the single mode fiber will have to be selected based on its very low, if not inexistent, self-induced fluorescence properties. There are also important advantages to using laser sources producing very short pulses if few meter range sensing is the scenario of interest.

Tilting the emission axis aside from the collection optical axis

A simple issue that should be pointed out is the possible obscuration of the emitted radiation by the fiber bundle mount.

Based on the schematic representation of the SR-BioSpectra concept found in Fig.1 and the anticipated low divergence of the irradiation emitted be the single mode fiber (see Section 3.3 and Chapter 4), an important fraction of the radiation fired at the probed cell may be blocked by the fiber bundle and its mount. One solution to efficiently avoid this difficulty is to slightly tilt the irradiation optical axis in comparison with the transmitter optical axis. This tilted design could be achieved mechanically in the design of the fiber bundle mount or with a fiber bundle specially design with intrinsic off axis emission. The angle of the off axis emission should be minimized while allowing most of the irradiation to exit the transmitter without hitting the fiber bundle mount. This off axis design should have little effect on the transmitter geometric form factor efficiency as long as the angle formed by the linear translation of the laser irradiation axis at the aperture stop and the range to the field stop is sufficiently small to keep the irradiation beam close to the transmitter optical axis in comparison with the diameter of the field stop within the field depth region.

The needs for improved electronic preprocessing: photon counting

In order to derive the sensitivity of the short-range spectrometric LIDARs reported in Chapter 4, a similar efficiency for the electronics of detection was assumed between the proposed SR-BioSpectra design and the SINBAHD system. This is reasonable since few hardware differences are anticipated between the two systems for the spectrometric detector and the processing unit. However, an important improvement in the function of these two components is envisaged under low

21 Elastic cross section of aerosol may be as high as a 1000 times higher than its inelastic counter part.

photonic signal conditions that would have a direct impact on enhancing the sensitivity of the device. This improvement is a result of the observation that, at low bioaerosol concentration, not all laser pulses fired at the probed cell will produce fluorescing photons (see the discussion about the volume of the probed cell in Chapter 4). That implies that not all fired laser pulses contribute to constructing the signal of interest while all acquisitions (with photon or not) contribute to raising the electronic noise floor.

One approach to drastically reduce this electronic noise contribution and substantially improve the noise floor limitation under low background radiance conditions (this is represented by the symbol Δ in Eq.27) is to preprocess each collected spectra. This preprocessing would involve the identification of photon detection events and their localization within the spectral interval of collection. Such processing for a single detected photon is possible with ICCD technology using a threshold algorithmic approach[22]. This will have the advantage of recording only the signal of interest (gated signals with detected photons) and discarding signals responsible for the electronic noise floor (gated signals having no photon detections). Nevertheless, such processing will be rendered worthless under strong photonic signals (of multiple origins) where the detection is photon shot noise limited. Furthermore, another limitation to this preprocessing approach will appear when the probability of having two photons within the same spectral bin is non-negligible. In addition to underestimating the collected signal, photon counting under this condition will contribute to degrading the quality of the spectral information.

Another reason supporting the need for preprocessing each collected fluorescent spectra is the rejection of fluorescence anomalies. Several causes can create this situation; for instance, macroscopic living organisms (i.e., flying insects) or solid materials temporarily crossing the probe cell are examples of such scenarios. Without preprocessing, fluorescence anomalies will force the rejection of the whole acquisition train while in fact only a few acquisitions needed to be discarded.

Understanding the sensitivity of a LIDAR biodetector expressed in ACPLA or ppl

A final important issue that should be discussed in this report is the unit expressing the sensitivity of a bioaerosol detector and how to interpret this quantified sensitivity with LIDAR technologies.

The sensitivity of a bioaerosol detector is usually expressed in ACPLA (Agent Containing Particles per Liter of Air) or in ppl (particles per liter). Expressing the concentration of a biological cloud in ACPLA has the advantage of describing its content in living units; this is equivalent to expressing the lethality of a cloud formed of bioagents. On the other hand, the ppl is a more basic unit reporting only the concentration of aerosols. Furthermore, ppl must be employed to characterize

22 It is common to obtain amplification levels with ICCD that make the amplitude of a single detected photon several times greater than the standard deviation of the noise associated with the electronics of the sensor.

bioaerosol clouds of large concentration where instruments reporting biocloud concentration in ACPLA cannot be used.

With these two units of concentration, the information on the size of the bioaerosol is not included. Size information has little impact on the measurement of the sensitivity of bioaerosol point sensors (even if the size of the bioaerosol is an important parameter measured by several of these sensors). Conversely, the size of the bioaerosol directly affects the sensitivity of standoff biodetector based on LIDAR technology. This size dependency is expressed as the projected area in the definition of the bioaerosol cross section (Eq.4). The implication of this relation means that a LIDAR reporting a given sensitivity in ppl or ACPLA under a given condition of acquisition (range, binning time, energy delivered…) may report a completely different sensitivity under the exact same conditions of acquisition but with a bioaerosol of a different size. As an example, the SINBAHD system reported a sensitivity of about 5 ACPLA at a range of 1.4 km during night conditions with BG as a simulant. This was obtained with bioaerosols having, on average, about 3 μm in diameter. If the produced bioaerosol cloud submitted to the SINBAHD system were instead made of military grade bioaerosol (military grade bioaerosols are designed to content a single biological agent), the size of the bioaerosol would have been about 1 μm in diameter. In this case, the sensitivity reported by the SINBAHD system under the same conditions would have been about 9 times higher (about 45 ACPLA) because of the projected area dependency. This emphasizes the importance of indicating the average size of the bioaerosol when reporting the sensitivity of a LIDAR in ACPLA, ppl, or any other units characterizing a bioaerosol volume concentration.

6. Conclusion

In order to characterize the sensitivity of short-range spectrometric LIDARs to detect bioaerosols from a standoff position, a working model is elaborated. The model is derived from fundamental principles associated with classical LIDAR theory that are adapted for short-range applications. To use a narrow field of view to reduce the background radiance contribution, a necessary condition for a robust bioaerosol detector based on LIDAR technology, a transmitter with its image plane located at the range of interest is proposed. To facilitate the use of this design, a combined source-collector module based on fibre bundle technology is identified as a key component of the transmitter. The optical design of the transmitter, including the irradiation geometry, is analyzed in depth to facilitate estimation of the geometric form factor, an important parameter dictating the LIDAR collection efficiency. Introducing the scattering properties of *Bacillius Globiggi* (BG) (an important simulant of biological agents) obtained from previous studies conducted under the SINBAHD project (a program investigating long-range bioaerosol detection based on a similar LIDAR technology), a sensitivity varying from less than 1 to about 80 ACPLA is anticipated for ranges varying from 5 to 50 m and collection apertures of 5, 10, 15 and 20 cm in diameter. To obtain this level of sensitivity, the probed range intervals (being the transmitter field depths), delimiting monitored atmospheric volumes varying from a fraction of a millilitre to about 60 mL, vary from less than .5 m to over 30 m. These results are supplemented with a discussion on issues such as the limit of validity of the proposed model, the modelling of background parasitic signals (usually dictating the sensitivity limit), the requirement for preprocessing the acquired spectra, possible parasitic fluorescence sources (an issue that must be overcome to achieve the reported sensitivity predictions), and how to interpret the concentration sensitivity of a bioaerosol detector based on LIDAR technology.

In summary, this projected capacity is applied to obtain a short-range bioaerosol detector based on LIDAR technology as the SR-BioSpectra. This concept is the subject of a report of invention filed by DRDC – Valcartier for monitoring large indoor and semi-enclosed outdoor spaces. Continued efforts to advance this technology should consist in experimental verification of the predicted sensitivity through the development of a breadboard demonstrator.

7. References

1. J.-R. Simard, G. Roy, P. Mathieu, V. Larochelle, J. McFee and J. Ho, “Standoff Integrated bioaerosol Active Hyperspectral Detection (SINBAHD): Final Report”, DREV-TR-2002-125, Nov 2002, 113 pages.
2. Jean-Robert Simard, Gilles Roy, Pierre Mathieu, Vincent Larochelle, John McFee, Jim Ho, “SR-BioSpectra”, report of an invention, DRDC Valcartier, October 2004.
3. R. M. Measures, “Laser Remote Sensing: Fundamentals and Applications”, John Wiley & Sons, Inc., Chap. 7, 1984.
4. Simard, J.R., Roy, G., Mathieu, P., Larochelle, V., McFee, J., Ho, J., “Standoff sensing of bioaerosols using intensified range-gated spectral analysis of laser-induced fluorescence”, IEEE Trans. on Geoscience and Remote Sensing, Vol. 42, No. 4, April 2004.
5. R. M. Measures, “Laser Remote Sensing: Fundamentals and Applications”, John Wiley & Sons, Inc., Sec. 7.4.1, 1984.
6. H. Kogelnik and T. Li., “Laser Beams and Resonators”, Applied Optics, Vol. 5, No. 10, IEEE Trans. on Geoscience and Remote Sensing, Vol. 42, No. 4, pp. 1550-1567, October 1966.

Distribution list

INTERNAL

DRDC Valcartier TM 2005-303

1 – Director General
3 – Document Library
1 – J.-R. Simard (author)
1 – Gilles Roy
1 – Pierre Mathieu
1 – Vincent Larochelle
1 – Sylvie Buteau
1 – Pierre Lahaie
1 – Bernard Déry
1 – Jean-Marc Garneau
1 – Jean-Marc Thériault
1 – Luc Bissonnette
1 – Hugo Lavoie
1 – Eldon Puckrin
1 – Julie Couet
1 – Farida Souiki

EXTERNAL

DRDC Valcartier TM 2005-303

1 – DRDKIM (PDF file)
1 – Director Science and Technology Maritime
1 – Director Science and Technology Land
1 – Director Science and Technology Air
1 – Director Science and Technology Human Performance
1 – Director Science and Technology Human Performance 3
1 – Directorate of Maritime Ship Support 4-2-3
1 – Director Marine Requirements Sea
1 – Director Land Requirements
1 – Director of Air Requirements
1 – Director Nuclear, Biological and Chemical Defence 2
1 – Director Nuclear, Biological and Chemical Defence 2-3
1 – John McFee, DRDC Suffield
1 – Jim Ho, DRDC Suffield
1 – Les Negata, H/CBDS, DRDC Suffield

DOCUMENT CONTROL DATA

1. ORIGINATOR (name and address)

Jean-Robert Simard, DRDC Valcartier, 2459 Pie XI Blvd North
Québec (Quebec), Canada, G3J 1X5

2. SECURITY CLASSIFICATION
(Including special warning terms if applicable)
UNCLASSIFIED

3. TITLE (Its classification should be indicated by the appropriate abbreviation (S, C, R or U)

Short-range bioaerosol LIDAR detection : transmitter design and sensitivity analysis (U)

4. AUTHORS (Last name, first name, middle initial. If military, show rank, e.g. Doe, Maj. John E.)
Simard, Jean-Robert

5. DATE OF PUBLICATION (month and year)
2006

6a. NO. OF PAGES
49

6b. NO. OF REFERENCES
6

7. DESCRIPTIVE NOTES (the category of the document, e.g. technical report, technical note or memorandum. Give the inclusive dates when a specific reporting period is covered.)
Technical Memorandum

8. SPONSORING ACTIVITY (name and address)
DRDC Valcartier

9a. PROJECT OR GRANT NO. (Please specify whether project or grant)
None

9b. CONTRACT NO.

10a. ORIGINATOR'S DOCUMENT NUMBER
TM 2005-303

10b. OTHER DOCUMENT NOS
N/A

11. DOCUMENT AVAILABILITY (any limitations on further dissemination of the document, other than those imposed by security classification)

- [X] Unlimited distribution
- [ ] Contractors in approved countries (specify)
- [ ] Canadian contractors (with need-to-know)
- [ ] Government (with need-to-know)
- [ ] Defense departments
- [ ] Other (please specify)

12. DOCUMENT ANNOUNCEMENT (any limitation to the bibliographic announcement of this document. This will normally correspond to the Document Availability (11). However, where further distribution (beyond the audience specified in 11) is possible, a wider announcement audience may be selected.)

Unlimited

13. ABSTRACT (a brief and factual summary of the document. It may also appear elsewhere in the body of the document itself. It is highly desirable that the abstract of classified documents be unclassified. Each paragraph of the abstract shall begin with an indication of the security classification of the information in the paragraph (unless the document itself is unclassified) represented as (S), (C), (R), or (U). It is not necessary to include here abstracts in both official languages unless the text is bilingual).

With the decline of the traditional worldwide balance of power between the major countries that occurred since the early '90s and the rise of asymmetric threats that was observed in parallel, biological warfare has been identified and still is one of the menaces for which adequate defenses are the most challenging. One need recently identified is a short-range volumetric bioaerosol sensor capable of monitoring large indoor and semi-enclosed outdoor spaces. In response to this interest, DRDC Valcartier has investigated the potential of a miniature inelastic short-range LIDAR (the Short-Range BioSpectra concept). In addition of addressing the identified deficiencies, such device would also accelerate the potential assessment of classifying biological aerosols from the spectral information contained in their induced fluorescence. Within this study, several modeling considerations necessary for an efficient short-range LIDAR transmitter design are reported. From this model, the present state of the technologies and previously obtained scattering properties of a bioaerosol stimulant (BG), sensitivities varying from less than 1 to about 80 ACPLA are anticipated for range varying from 5 to 50 meters and collecting apertures of 5, 10, 15 and 20 cm in diameter. This level of sensitivity is obtained for probed range intervals of less than half meter to more than 30 meters, delimiting atmospheric volumes varying from a fraction of milliliter to about 60 milliliter. These results are supplemented with discussions on issues like the limit of validity of the proposed model, the modeling of background parasitic signal, preprocessing requirements, possible parasitic fluorescence sources (a paramount issue to overcome in order to achieve the reported sensitivity predictions) and how to interpret the concentration sensitivity of a bioaerosol detector based on LIDAR technology.

14. KEYWORDS, DESCRIPTORS or IDENTIFIERS (technically meaningful terms or short phrases that characterize a document and could be helpful in cataloguing the document. They should be selected so that no security classification is required. Identifiers, such as equipment model designation, trade name, military project code name, geographic location may also be included. If possible keywords should be selected from a published thesaurus, e.g. Thesaurus of Engineering and Scientific Terms (TEST) and that thesaurus-identified. If it is not possible to select indexing terms which are Unclassified, the classification of each should be indicated as with the title.)

Bioaerosol, Detection, Classification, LIF, LIDAR, short-range, spectral signature, transmitter design

Defence R&D Canada

Canada's Leader in Defence
and National Security
Science and Technology

R & D pour la défense Canada

Chef de file au Canada en matière
de science et de technologie pour
la défense et la sécurité nationale

WWW.drdc-rddc.gc.ca